JOURNAL OF SANDWICH STRUCTURES & MATERIALS

Original Article

Journal of Sandwich Structures and Materials
0(00) 1–37

DOI: 10.1177/1099636217727801
journals.sagepub.com/home/jsm
SAGE

A modified state space differential quadrature method for free vibration analysis of soft-core sandwich panels

Balavishnu Udayakumar and KV Nagendra Gopal

Abstract

Modifications and improvements to conventional state space differential quadrature method are proposed for free vibration analysis of thick, soft-core sandwich panels with arbitrary edge boundary conditions, using an exact two-dimensional elasticity model. The modifications are based on a systematic procedure to implement all possible combinations of edge boundary conditions including simply supported, clamped, free and guided edges. Natural frequencies and mode shapes are obtained and compared with exact elasticity solutions from state space method and approximate solution from finite element simulations; demonstrating the high numerical accuracy and rapid convergence of the modified method. Further, the proposed framework is compared to the conventional implementation of the state space differential quadrature method for thick cantilever sandwich panels and is shown to give results with better accuracy and faster convergence.

Keywords

Modified state space differential quadrature method, soft-core sandwich panels, exact elasticity models, arbitrary edge boundary conditions, free vibration

Introduction

Sandwich constructions, typically including two outer face sheets separated by a relatively thick, low density and compliant core, are crucial in the design of high performance and cost effective aerospace, automobile and marine structures due

Department of Aerospace Engineering, Indian Institute of Technology Madras, Chennai, India

Corresponding author:
KV Nagendra Gopal, Department of Aerospace Engineering, Indian Institute of Technology Madras, Chennai 600036, India.
Email: gopal@iitm.ac.in

to its high specific strength and bending stiffness, damage tolerance, buckling resistance and energy absorption capabilities [1–3]. Advanced materials like laminated or particulate composites, functionally graded or multi-functional materials are used by designers to tailor, optimize or include multi-functionality to the sandwich structure.

The conventional approximate theories used for modeling sandwich panels include physically justifiable approximations in the stress or displacement field when modeling the face sheet and/or the core [4–6]. The displacement-based approximate models fall under two broad categories: the equivalent single layer (ESL) models and the layer-wise (LW) models [7]. When using such approximate models, there are two parameters that can significantly affect the accuracy of the solution; namely, the relative stiffness of the face sheet with respect to the core and the length-to-thickness ratio of the panel. It has been observed that for a high value of the former parameter (i.e. a soft-core sandwich panel) the ESL models fail to provide acceptable results [8].

In soft-core sandwich panels, there can be significant transverse deformations in the core under impulsive and localized dynamic loads. A specialized approximate model, based on the high-order sandwich panel theory (HSAPT) [9], was developed to capture these localized effects and used for free vibration analysis [10,11]. Recently, an extended high-order sandwich panel theory (EHSAPT) was proposed to include the effects of in-plane rigidity of the core [12]. The natural frequencies and mode shapes of simply supported sandwich panels with compressible and incompressible cores were obtained using the ESL, HSAPT and EHSAPT models and compared with two-dimensional elasticity results as benchmark [13,14]. Unlike the conventional incompressible models, the high-order models could detect the displacement eigenmodes along the length and through the thickness of the panel for higher modes. In soft-core sandwich panels, except for the difference in the mode shapes of the third and the fifth transverse displacements corresponding to the first wave number, the results given by EHSAPT matched with that of the benchmark elasticity results. These models were also used for free vibration analysis of soft-core sandwich structures with different boundary conditions [15,16]. Although such plate theory models are suited for specific problems, they should be validated against exact elasticity models, especially for edge boundary conditions other than the simply supported case.

Exact solutions for elasticity models are limited to cases with simply supported edge conditions, special material symmetries and regular geometries [17–22]. For other cases, approximate solution of exact elasticity model is needed to develop benchmark results. However, accuracy and convergence of the solution methodology need to be ensured.

Commonly used analytical approaches for solving elasticity models can be classified under one of these methods: viz. Pagano's approach, state space method (SSM), series expansion approach and asymptotic approach [23]. Of these, SSM is particularly suited to obtain exact solutions for small deformation linear elastic response of multi-layered structures modelled as continuum [24–26]. Due to its

inherent limitation in solving problems involving arbitrary edge boundary conditions and geometry, semi-analytical methods based on the state space formulation were developed in combination with existing numerical methods like the finite difference, finite element, boundary element and differential quadrature method (DQM) [27–30]. Compared to the conventional lower order numerical methods, the DQM provides computationally efficient and numerically accurate solutions with small number of grid points and is therefore well suited for structural vibration analysis [31,32].

The state space differential quadrature method (SSDQM) was developed to combine the advantages of the SSM and DQM [33]. This has been used for free vibration analysis of multi-layered beams [33] and rectangular plates [34–36]. The advantage of SSDQM is that the thickness variation of field variables can be obtained analytically using SSM while in-plane dependence can be numerically solved using DQM for different edge boundary conditions. But when the number of grid points are increased, the conventional transfer matrix approach of the SSDQM [33–35] leads to numerical instabilities, especially for higher frequencies. This is due to multiplication of the local transfer matrices of different layers leading to the accumulation of numerical errors. An effective way to avoid this is to assemble the local transfer matrices to obtain the global transfer matrix [36]. It should be noted that, even in this approach, instabilities can occur when a single set of grid points along the in-plane direction, in the computational domain, is used to represent a thick layer in the multi-layered structure. But this can easily be overcome by dividing the thick layer into sufficient number of artificial layers along the thickness co-ordinate.

From literature, it is observed that the studies based on exact elasticity models are mostly limited to sandwich panels with simply supported edges. For thick, soft-core panels, the specialized models failed to capture some of the higher mode shapes of transverse displacement. Thus, there is a need to develop exact or accurate approximate solutions using exact elasticity models for thick panels with arbitrary edge boundary conditions. The SSDQM is particularly suited for this task. However, proper convergence studies are needed for each edge boundary condition and modes of vibration. Even in the reported studies using SSDQM, the mode shapes corresponding to different natural frequencies are not explicitly identified and convergence studies are limited to few cases. Moreover, no study using SSDQM is found on panels with guided edge boundary condition.

The present work provides benchmark results based on two-dimensional exact elasticity model for thick soft-core sandwich panels with arbitrary edge boundary conditions. New results, based on exact elasticity solutions using trigonometric functions, for panels with combination of simply supported and guided, are obtained. A systematic procedure is proposed for implementing all combinations of edge boundary conditions in the state space differential quadrature framework. The presented results include comparison with the conventional SSDQM formulation (refer Appendix A [33]), which show that the proposed modifications lead to a more general framework in implementing all combinations of edge boundary conditions and is also shown to give better numerical accuracy and faster convergence for thick,

cantilevered sandwich panels. The accuracy and convergence of the modified SSDQM procedure is demonstrated using thick, soft-core sandwich panels as test cases, before presenting the natural frequencies and the mode shapes. All the obtained results are compared by authors using finite element simulation.

State space differential quadrature formulation

State space formulation in plane elasticity

In the framework of two-dimensional linear elasticity, the equilibrium equations in the absence of body forces, the strain–displacement relations and the material constitutive law for each layer of a typical three-layered sandwich panel made of special orthotropic layers are given below

$$\begin{bmatrix} \partial_x & 0 & \partial_z \\ 0 & \partial_z & \partial_x \end{bmatrix} \begin{Bmatrix} \sigma_x \\ \sigma_z \\ \tau_{xz} \end{Bmatrix}^{(t,c,b)} = \begin{Bmatrix} \rho\, u_{,tt} \\ \rho\, w_{,tt} \end{Bmatrix}^{(t,c,b)} \tag{1}$$

$$\begin{Bmatrix} \epsilon_x \\ \epsilon_z \\ \gamma_{xz} \end{Bmatrix}^{(t,c,b)} = \begin{Bmatrix} u_{,x} \\ w_{,z} \\ u_{,z} + w_{,x} \end{Bmatrix}^{(t,c,b)} \tag{2}$$

$$\begin{Bmatrix} \sigma_x \\ \sigma_z \\ \tau_{xz} \end{Bmatrix}^{(t,c,b)} = \begin{bmatrix} C_{11} & C_{13} & 0 \\ C_{13} & C_{33} & 0 \\ 0 & 0 & C_{55} \end{bmatrix}^{(t,c,b)} \begin{Bmatrix} \epsilon_x \\ \epsilon_z \\ \gamma_{xz} \end{Bmatrix}^{(t,c,b)} \tag{3}$$

Here, σ, ϵ correspond to the normal stress and the normal strain, τ, γ to the shear stress and the engineering shear strain, u, w to the in-plane and the transverse displacements, C_{ij} to elements of stiffness matrix and ρ to the material density. The superscripts (t, c, b) refer, respectively, to the top face sheet, the core and the bottom face sheet layers. The symbols ∂_x or $()_{,x}$, ∂_z or $()_{,z}$ and $()_{,t}$ represent the partial derivatives with respect to the variables x, z and t, respectively.

Equations (1) to (3) are combined and re-arranged to derive the mixed form of elasticity equations with displacements and the transverse stresses as primary variables. These equations are written in the non-dimensional form as in equation (5) for harmonic motion using the following relations

$$\begin{Bmatrix} u \\ \sigma_z \\ w \\ \tau_{xz} \\ \sigma_x \end{Bmatrix} = \begin{Bmatrix} \mathrm{H}\,\bar{u} \\ C_{55}^{(b)}\sigma_\eta \\ \mathrm{H}\,\bar{w} \\ C_{55}^{(b)}\tau \\ C_{55}^{(b)}\sigma_\xi \end{Bmatrix} e^{i\omega t}, \quad \xi = \frac{x}{\mathrm{L}}, \quad \eta = \frac{z}{\mathrm{H}}, \quad \lambda = \frac{\mathrm{H}}{\mathrm{L}}, \quad \Omega = \omega \mathrm{H}\sqrt{\frac{\rho^{(b)}}{C_{55}^{(b)}}} \tag{4}$$

In the above relation, ξ and η are the normalized in-plane and transverse coordinates, $\bar{u}$, $\bar{w}$, σ_η, τ are the non-dimensional displacements and stresses, λ is the thickness-to-length ratio of the panel, ω and Ω are the circular natural frequency and non-dimensional frequency, respectively. The stresses and the frequency are non-dimensionalized using the material properties of the bottom layer.

The state equations, represented in matrix form for each layer of the sandwich panel, are given below

$$\begin{Bmatrix} \bar{u} \\ \sigma_\eta \\ \bar{w} \\ \tau \end{Bmatrix}^{(t,c,b)}_{,\eta} = \begin{bmatrix} \mathbf{0} & \mathbf{A} \\ \mathbf{B} & \mathbf{0} \end{bmatrix}^{(t,c,b)} \begin{Bmatrix} \bar{u} \\ \sigma_\eta \\ \bar{w} \\ \tau \end{Bmatrix}^{(t,c,b)} \tag{5}$$

The in-plane stress (derived variable) is related to the state variables as shown below

$$\sigma_\xi^{(t,c,b)} = \begin{bmatrix} \left(C_{11} - \frac{C_{13}^2}{C_{33}}\right) \frac{\lambda}{C_{55}^{(b)}} \partial_\xi & \frac{C_{13}}{C_{33}} & 0 & 0 \end{bmatrix}^{(t,c,b)} \begin{Bmatrix} \bar{u} \\ \sigma_\eta \\ \bar{w} \\ \tau \end{Bmatrix}^{(t,c,b)} \tag{6}$$

These equations are listed in detail in Appendix 1 (see equations (22) and (23)) along with sub-matrices **A** and **B** (refer equation (24)).

Discretization using DQM

In the set of state equations (refer equation (22) in Appendix 1), the derivatives with respect to the in-plane direction (ξ) can be discretized using the DQM. Thus, the derivative of any state variable with respect to ξ at a particular grid point in the computational domain is represented as a weighted sum of the state variable values at all the grid points along ξ co-ordinate direction. The grid distribution used is the Chebyshev-Gauss-Lobatto grids, a non-uniform cosine grid distribution, with closely spaced grid points towards edge boundaries, reported to give better accuracy compared to other type of grids [32].

The state equation (5) is discretized and its values at all the grid points are represented in matrix form as follows [33]

$$\begin{Bmatrix} \bar{\mathbf{u}} \\ \boldsymbol{\sigma}_\eta \\ \bar{\mathbf{w}} \\ \boldsymbol{\tau} \end{Bmatrix}^{(t,c,b)}_{,\eta} = \begin{bmatrix} \mathbf{0} & \mathbf{E} \\ \mathbf{F} & \mathbf{0} \end{bmatrix}^{(t,c,b)} \begin{Bmatrix} \bar{\mathbf{u}} \\ \boldsymbol{\sigma}_\eta \\ \bar{\mathbf{w}} \\ \boldsymbol{\tau} \end{Bmatrix}^{(t,c,b)} \tag{7}$$

Similarly, the derived variables are given as

$$\boldsymbol{\sigma}_{\xi}^{(t,c,b)} = \left[\left(C_{11} - \frac{C_{13}^2}{C_{33}} \right) \frac{\lambda}{C_{55}^{(b)}} \mathbf{X}^{(1)} \quad \frac{C_{13}}{C_{33}} \mathbf{I} \quad \mathbf{0} \quad \mathbf{0} \right]^{(t,c,b)} \begin{Bmatrix} \bar{\mathbf{u}} \\ \boldsymbol{\sigma}_{\eta} \\ \bar{\mathbf{w}} \\ \boldsymbol{\tau} \end{Bmatrix}^{(t,c,b)} \tag{8}$$

The components in bold face represent vectors or matrices. The sub-matrices **E** and **F** and all the equations from the above matrix are separately listed using index notation in Appendix 1 (equations (26) to (28)) for further clarity.

Solution methodologies

The edge boundary conditions such as simply supported (shear diaphragm type) (S), clamped (C), free (F) and guided (G) in terms of the state variables or the derived variable at $\xi = 0$ or 1 are given below

$$\begin{aligned} &\mathrm{S} : \bar{w} = 0, \sigma_{\xi} = 0 \quad \mathrm{C} : \bar{u} = 0, \bar{w} = 0 \\ &\mathrm{F} : \tau = 0, \sigma_{\xi} = 0 \quad \mathrm{G} : \bar{u} = 0, \tau = 0 \end{aligned} \tag{9}$$

Exact solutions using SSM

Exact solutions exist for sandwich panels with both edges simply supported, guided and combination of simply supported and guided. The state variables expanded in trigonometric series can be assumed as solutions for these types of boundary conditions as in equation (10). If instead of SG, GS is considered in equation (10), then the *sin*() changes to *cos*() and vice versa.

$$\begin{Bmatrix} \bar{u} \\ \sigma_{\eta} \\ \bar{w} \\ \tau \end{Bmatrix}_{\mathrm{SS}}^{(t,c,b)} = \sum_{m=0}^{\infty} \begin{Bmatrix} U_m \cos(m\pi\xi) \\ Z_m \sin(m\pi\xi) \\ W_m \sin(m\pi\xi) \\ R_m \cos(m\pi\xi) \end{Bmatrix}^{(t,c,b)}, \quad \begin{Bmatrix} \bar{u} \\ \sigma_{\eta} \\ \bar{w} \\ \tau \end{Bmatrix}_{\mathrm{GG}}^{(t,c,b)} = \sum_{m=0}^{\infty} \begin{Bmatrix} U_m \sin(m\pi\xi) \\ Z_m \cos(m\pi\xi) \\ W_m \cos(m\pi\xi) \\ R_m \sin(m\pi\xi) \end{Bmatrix}^{(t,c,b)}$$
$$\begin{Bmatrix} \bar{u} \\ \sigma_{\eta} \\ \bar{w} \\ \tau \end{Bmatrix}_{\mathrm{SG}}^{(t,c,b)} = \sum_{m=1}^{\infty} \begin{Bmatrix} U_m \cos((2m-1)\frac{\pi}{2}\xi) \\ Z_m \sin((2m-1)\frac{\pi}{2}\xi) \\ W_m \sin((2m-1)\frac{\pi}{2}\xi) \\ R_m \cos((2m-1)\frac{\pi}{2}\xi) \end{Bmatrix}^{(t,c,b)} \tag{10}$$

It can be observed that for each case, the assumed series solution in equation (10) satisfies the respective boundary condition given in equation (9) and the state vector equations in equation (5). By substituting each of these in equation (5),

the state equations for respective edge boundary conditions can be obtained. These when separated out specific to a particular wave number "m" lead to the following matrix equation

$$\begin{Bmatrix} U_m \\ Z_m \\ W_m \\ R_m \end{Bmatrix}^{(t,c,b)}_{,\eta} = \begin{bmatrix} \mathbf{0} & \overline{\mathbf{A}} \\ \overline{\mathbf{B}} & \mathbf{0} \end{bmatrix}^{(t,c,b)} \begin{Bmatrix} U_m \\ Z_m \\ W_m \\ R_m \end{Bmatrix}^{(t,c,b)} \tag{11}$$

where $\overline{\mathbf{A}}$ and $\overline{\mathbf{B}}$ are given in Appendix 1 for SS, GG and SG cases.

Following the conventional transfer matrix approach [33] and implementing the traction-free boundary conditions at the lateral edges, the following relation is obtained.

$$\begin{Bmatrix} 0 \\ 0 \end{Bmatrix}^{(t)}_{(h)} = \left[\overline{\mathrm{T}}_m \right] \begin{Bmatrix} U_m \\ W_m \end{Bmatrix}^{(b)}_{(0)} \tag{12}$$

The non-trivial solution for equation (12) is

$$\det\left(\left[\overline{\mathrm{T}}_m \right] \right) = 0 \tag{13}$$

The above equation is a transcendental equation in "Ω_m", which gives infinite solutions for each value of the wave number "m."

It should be noted that $m = 0$ also gives different modes of vibration for SS and GG cases. On substituting $m = 0$ in equation (10) and following similar procedures from equations (11) to (13), the frequencies for $m = 0$ can be obtained. But $m = \frac{1}{2}$ does not correspond to a possible solution for SG or GS cases as it, respectively, leads to a non-zero value of $\bar{u}$ or $\bar{w}$ at $\xi = 1$ violating the edge boundary condition for guided or simply supported case.

Approximate solutions using SSDQM

In conventional SSDQM [33], the edge boundary conditions are implemented into the discretized governing equations (equation (27) in Appendix 1) in a trial and error manner for different cases, without providing a general framework applicable for all combinations of edge boundary conditions (refer Appendix A [33]). The global transfer matrix in this conventional implementation is obtained by multiplication of the local transfer matrices, followed by the enforcement of the traction-free conditions at lateral edges, leading to the frequency equation

$$\begin{Bmatrix} \mathbf{0} \\ \mathbf{0} \end{Bmatrix}^{(t)}_{(h)} = \overline{\mathbf{T}} \begin{Bmatrix} \mathbf{u} \\ \mathbf{w} \end{Bmatrix}^{(b)}_{(0)} \tag{14}$$

$$\det(\overline{\mathbf{T}}) = 0 \tag{15}$$

where $\mathbf{u}$ and $\mathbf{w}$ are vectors and $\overline{\mathbf{T}}$ is a sub-matrix of the global transfer matrix. However, the conventional method using the multiplication of local transfer matrices results in numerical instabilities and hence a different approach is used to obtain the global transfer matrix by assembling the local transfer matrices [36]. In this work, we propose a general procedure for implementing any combination of edge boundary conditions.

A systematic method to implement arbitrary edge boundary conditions. The discretized state equations should be re-formulated based on the edge boundary conditions before implementing the transfer matrix relations as explained further.

First, as all the transfer matrix relations and interface continuity conditions have to be expressed in terms of the state variables, any edge boundary condition specified in terms of the derived variable (σ_ξ) is converted in terms of the state variables using equation (28) (refer Appendix 1). Consider the example of a simply supported or a free edge panel where $\sigma_\xi = 0$ at $\xi = 1$ and/or N, leads to the following relation

$$\mathrm{A_{XX}} \sum_{j=1}^{N} X_{ij}^{(1)} \bar{u}_j + \frac{C_{13}^{(b)}}{C_{33}} \sigma_{\eta i} = 0, \quad i = 1 \text{ and/or } N \tag{16}$$

From this equation, any of the three state variables at the edges, namely, $\bar{u}_1$, $\bar{u}_N$, and $\sigma_{\eta 1}$ or $\sigma_{\eta N}$, depending on whether the edge condition is $\sigma_{\xi 1} = 0$ (for $\sigma_{\eta 1}$) or $\sigma_{\xi N} = 0$ (for $\sigma_{\eta N}$) respectively, can be written in terms of the other two. For example, if $\xi = 1$ is simply supported, $\sigma_{\xi N} = 0$ condition can be used to obtain the relation of $\sigma_{\eta N}$ with $\bar{u}_1$ and $\bar{u}_N$ and therefore $\sigma_{\eta N}$ need not be included in the equations to be solved (see equation (29) in Appendix 1).

Next, as the final step in the free vibration analysis involves computing the determinant of the sub-matrix in the frequency equation for the conventional transfer matrix approach (see equation (15)) or that of an assembled matrix $\left[\mathbf{JT}\right]$ (see equation (21)), it is necessary that enforcing of the edge boundary conditions should lead to square matrices. But for several cases, for example the clamped-clamped (CC) boundary condition, it can be observed that for the conventional transfer matrix approach, the order of the sub-matrix $\overline{\mathbf{T}}$ in equation (14) is $(2N, 2(N-2))$ when the primary boundary conditions (those directly given by equations (9)) $\bar{u}_1 = 0$, $\bar{u}_N = 0$, $\bar{w}_1 = 0$ and $\bar{w}_N = 0$ alone are implemented. Further in the assembled transfer matrix approach, implementing the primary edge boundary conditions alone leads to a non-square matrix $\left[\mathbf{JT}\right]$ in equation (21). These can be avoided by observing that for CC case both the displacement variables (u and w) are zero all along the edges ($\xi = 0$ and $\xi = 1$) and hence their derivatives with respect to the transverse co-ordinate 'η' at these edges are also zero. Making use of these conditions in the first and third set of state equations in equation (27) (see Appendix 1), the values of the state variables τ_1, τ_N and $\sigma_{\eta 1}$, $\sigma_{\eta N}$

become known in terms of $\bar{w}_i$ and $\bar{u}_i$ respectively, $i = 2, \ldots, N-1$. Avoiding these known state variables from the set of equations to be solved, a square sub-matrix of order $(2(N-2), 2(N-2))$ is obtained in equation (15); and also $\left[\mathbf{JT}\right]$ in equation (21) becomes square. The details of equations after implementing CC boundary condition can be referred in equation (32).

On generalizing this idea, it can be concluded that substitution of the primary boundary conditions in the governing state equations can provide the derived secondary boundary conditions which can be used when necessary. But care should be taken to include the derived conditions only after implementing the primary boundary conditions. For example, in SS case, the values for $\sigma_{\eta 1}$ and $\sigma_{\eta N}$ are obtained from the primary conditions $\sigma_{\xi 1} = 0$ and $\sigma_{\xi N} = 0$ rather than deriving them from $\bar{w}_1 = 0$ and $\bar{w}_N = 0$ for the same (refer equation (29) in Appendix 1).

Based on these observations, changes in the procedure for implementing CF edge boundary condition, from that of the conventional procedure (refer Appendix A [33]), are proposed. Although the conventional method for implementing CF edge condition were mathematically correct, it is found that the modified formulation gives better numerical accuracy and faster convergence for all modes of vibration (refer Table 5). Therefore, here, the primary boundary conditions $\bar{u}_1 = 0$, $\bar{w}_1 = 0$, and $\tau_N = 0$ and the derived conditions for τ_1 and $\sigma_{\eta 1}$ (respectively from $\bar{u}_1 = 0$ and $\bar{w}_1 = 0$ conditions), obtained following similar procedures as explained earlier, along with the relation of $\bar{u}_N$ obtained from $\sigma_{\xi N} = 0$ are used for enforcing the boundary conditions for CF panel (refer equation (33) in Appendix 1).

It can be seen from the above discussion that every combination of edge boundary conditions can be enforced in a simple systematic manner if the state vector pairs $\bar{u}$ and τ, $\bar{w}$ and σ_η are, respectively, of the same size with conditions (primary or secondary) specified on the same edge (or edges) for each one in a particular pair. This can eliminate all the mentioned issues and provide better accuracy and convergence for SSDQM. The same idea is conveyed in Table 1. Here, for each case of edge boundary conditions, the variables whose numerical values are zero at the edges (representing the primary boundary conditions) and those with known values (the secondary conditions derived from the primary boundary conditions) are, respectively, represented as "0" and "✓". It can immediately be noted from Table 1 that, as previously mentioned, the state vector pairs $\bar{u}$ and τ, $\bar{w}$ and σ_η are, respectively, of the same size for all the cases. Also similar conditions are specified on the same edge (or edges) for each one in a particular pair for all cases. For example, referring to the CF case (see Table 1 and equations (33) for clarity), the state vectors $\mathbf{u}$ and $\boldsymbol{\tau}$ have same size $((N-2) \times 1)$ and so do $\mathbf{w}$ and $\boldsymbol{\sigma}_\eta$ $((N-1) \times 1)$. Moreover, the primary condition for $\mathbf{w}$ ($w_1 = 0$) and secondary condition for $\boldsymbol{\sigma}_\eta$ ($\sigma_{\eta 1}$ known from $w_1 = 0$) are specified on the same edge $\xi = 0$; this being contrary to the procedure followed in conventional SSDQM (see Appendix A [33]).

The set of state equations after implementing the edge boundary conditions for all possible combinations of simply supported, clamped, free and guided edges using the proposed methodology are listed in Appendix 1 (see equations (29) to (38)).

Table 1. A schematic of the procedure followed in implementing different boundary conditions.

	u_1	u_N	$\sigma_{\eta 1}$	$\sigma_{\eta N}$	w_1	w_N	τ_1	τ_N	$\sigma_{\xi 1}$	$\sigma_{\xi N}$
SS			✓	✓	0	0			0	0
GG	0	0					0	0		
SG		0	✓		0			0	0	
CC	0	0	✓	✓	0	0	✓	✓		
CF	0	✓	✓		0		✓	0		0
FF	✓	✓					0	0	0	0
CS	0		✓	✓	0	0	✓			0
SF		✓	✓		0			0	0	0
CG	0	0	✓		0		✓	0		
FG	✓	0					0	0	0	

Developing the global transfer matrix

After implementing the edge boundary conditions, the discretized state equations for any case can be written in the following form

$$\begin{Bmatrix} \overline{\mathbf{u}} \\ \boldsymbol{\sigma}_\eta \\ \overline{\mathbf{w}} \\ \boldsymbol{\tau} \end{Bmatrix}^{(t,c,b)}_{,\eta} = \begin{bmatrix} \overline{\mathbf{0}} & \overline{\mathbf{E}} \\ \overline{\mathbf{F}} & \overline{\mathbf{0}} \end{bmatrix}^{(t,c,b)} \begin{Bmatrix} \overline{\mathbf{u}} \\ \boldsymbol{\sigma}_\eta \\ \overline{\mathbf{w}} \\ \boldsymbol{\tau} \end{Bmatrix}^{(t,c,b)} \tag{17}$$

It should be noted that the size of the state vectors and the coefficient matrices in the above equations differ with the type of edge boundary conditions of the panel.

To avoid multiplication, the local transfer matrices are assembled to obtain the global transfer matrix [36]. This leads to the following relation

$$\boldsymbol{\delta} = \mathbf{T}\boldsymbol{\delta}_0 \tag{18}$$

where $\mathbf{T}$ is the global transfer matrix.

Also assembling the interface continuity and loading conditions gives

$$\mathbf{J}\boldsymbol{\delta} = \mathbf{f} \tag{19}$$

The details of vectors $\boldsymbol{\delta}_0$, $\boldsymbol{\delta}$, $\mathbf{f}$ and matrices $\mathbf{T}$, $\mathbf{J}$ are given in Appendix 1 (see equations (39) and (40)).

Substituting equation (18) in equation (19) gives

$$\mathbf{JT}\boldsymbol{\delta}_0 = \mathbf{f} \tag{20}$$

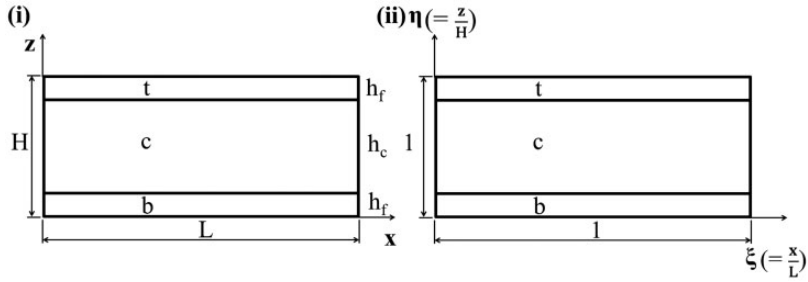

Figure 1. (i) and (ii) are schematic of the sandwich panel, respectively, in physical and normalized coordinate systems (not drawn to scale). The letters t, c and b denote, respectively, the top face sheet, core and the bottom face sheet. Refer Table 2 for details of material and geometric parameters of this sandwich panel.

Table 2. Material and geometric parameters of the sandwich panel considered for present study [13].

H(mm)	L(mm)	h_f (mm)	h_c (mm)	$\frac{L}{H}$
48	152.4	5	38	3.1750
E_f (GPa)	E_c (GPa)	ρ_f (kg m^{-3})	ρ_c (kg m^{-3})	μ_f, μ_c
13.6	0.032	1800	58.5	0.25

Table 3. Convergence of natural frequencies (Hz) using SSDQM for SS, GG and SG edge boundary conditions.

	$N=5$	$N=7$	$N=9$	$N=11$	$N=13$	$N=15$	$N=17$	SSM
SS/GG								
a = 1	620.86	622.56	622.56					$622.56^{(1,1)}$
t = 1	2277.10	2277.00	2277.00					$2277.00^{(1,2)}$
a = 2		1527.53	1526.61	1526.56	1526.56			$1526.56^{(2,1)}$
t = 2		2432.77	2432.39	2432.37	2432.37			$2432.37^{(2,2)}$
a = 4				4632.87	4628.41	4628.46	4628.46	$4628.46^{(4,1)}$
t = 4				4829.13	4824.97	4825.01	4825.01	$4825.01^{(4,2)}$
SG								
a = 1	283.17	283.17	283.17					$283.17^{(1,1)}$
t = 1	2280.12	2292.26	2292.25					$2292.25^{(2,2)}$
a = 2		1028.84	1028.80	1028.80	1028.80			$1028.80^{(2,1)}$
t = 2		2312.09	2312.09	2312.09	2312.09			$2312.09^{(1,2)}$
a = 4				3676.47	3679.39	3679.37	3679.37	$3679.37^{(4,1)}$
t = 4				3959.62	3962.20	3962.18	3962.18	$3962.18^{(4,2)}$

Table 4. Convergence of natural frequencies (Hz) using SSDQM for different combinations of edge boundary conditions.

	Mode	$N=7$	$N=11$	$N=17$	$N=23$	$N=25$	$N=27$	FEM
CC	a = 1	858.19	854.37	853.49	853.33	853.32		853.37
	t = 1	2369.77	2369.37	2369.30	2369.27	2369.27		2369.3
	a = 4			5566.19	5564.96	5564.81	5564.71	5565.4
CF	a = 1	333.11	330.19	329.97	329.90	329.89		329.88
	t = 1	2275.95	2276.63	2276.37	2276.30	2276.29		2276.3
	a = 4			3694.23	3694.47	3694.58	3694.66	3695.2
FF	a = 1	1315.96	1303.79	1303.10	1303.03	1303.03		1303.0
	t = 1	2246.04	2246.35	2246.13	2246.06	2246.05		2246.1
	a = 4			3827.21	3827.08	3827.06	3827.05	3827.1
CS	a = 1	725.67	724.02	723.60	723.53	723.52		723.53
	t = 1	2302.06	2302.04	2302.02	2302.01	2302.01		2302.0
	a = 4			5085.85	5085.34	5085.28	5085.23	5085.5
SF	a = 1	886.65	885.63	885.55	885.54	885.54		885.54
	t = 1	2256.21	2257.46	2257.45	2257.42	2257.41		2257.4
	a = 4			3333.42	3333.36	3333.35	3333.35	3333.4
CG	a = 1	340.39	339.82	339.69	339.67	339.67		339.68
	t = 1	2311.47	2311.46	2311.45	2311.45	2311.45		2311.4
	a = 4			4081.78	4081.35	4081.30	4081.26	4081.5
FG	a = 1	590.23	589.16	589.09	589.09	589.09		589.09
	t = 1	2256.58	2256.98	2256.81	2256.76	2256.75		2256.8
	a = 4			4204.83	4204.76	4204.75	4204.75	4204.8

For free vibration analysis, $\mathbf{f} = \mathbf{0}$, which implies equation (20) is homogeneous and so for non-trivial solution

$$\det(\mathbf{JT}) = 0 \tag{21}$$

The above determinant gives a transcendental equation in Ω, which when solved numerically gives all the frequencies of all the modes for a particular combination of edge boundary condition.

Results and discussion

In this section, 'SSDQM' refers to the state space differential quadrature method including the proposed modifications. The proposed methodology has been implemented in MATLAB®. The sandwich panel, under present study (see the schematic in Figure 1), consist of three layers of isotropic materials – two face sheets and a core; all of which are modelled using the material constitutive law for 2D elasticity

Table 5. Convergence of natural frequencies (Hz) using conventional (CON) [33] and modified (MOD) SSDQM for sandwich panel with CF edge boundary condition.

Mode		$N=7$	$N=11$	$N=17$	$N=23$	$N=25$	$N=27$	FEM
1 (a_1)	MOD	333.1	330.2	330.0	329.9	329.9		329.9
	CON	329.1	329.9	330.1	330.0	330.0		
2 (a_2)	MOD	1098.0	1092.7	1092.3	1092.4	1092.4		1092.6
	CON	1135.7	1121.6	1106.4	1099.7	1098.5		
3 (a_3)	MOD	2152.5	2182.8	2180.2	2179.5	2179.4	2179.3	2179.2
	CON	2201.7	2193.0	2195.0	2188.5	2187.1	2185.9	
4 (t_1)	MOD	2276.0	2276.6	2276.4	2276.3	2276.3		2276.3
	CON	2301.2	2300.8	2299.5	2295.2	2293.3		
5 (t_2)	MOD	2310.3	2310.6	2310.7	2310.7	2310.7		2310.8
	CON	2392.9	2386.0	2347.3	2323.9	2320.2		
6 (t_3)	MOD	2760.2	2785.2	2784.1	2783.6	2783.5	2783.5	2783.3
	CON	2840.3	2843.7	2812.7	2796.8	2794.0	2792.0	

FEM: finite element method.

plane strain condition (see equation (41) in Appendix 1). Its geometric and material properties are given in Table 2, where subscripts '*f*' and '*c*', respectively, denote variables corresponding to face sheets and core. Exact elasticity solutions for natural frequencies and mode shapes are obtained using SSM for SS, GG and SG panels. These results are used to validate the numerical accuracy of SSDQM for those cases. For cases where exact solutions are not possible, the results obtained using SSDQM are compared with those from finite element analyses using commercial software Abaqus®. In the finite element model, the face sheets and the core are meshed with eight-noded bi-quadratic plane strain quadrilateral elements with reduced integration.

Convergence studies

The convergence of SSDQM for SS, GG and SG panels are presented in Table 3. Exact solutions for each of these cases, obtained using SSM, are listed along with the SSDQM numerical results. It can be noticed that the SSM results are superscripted with two numbers in parentheses separated by a comma. The first digit is the wave number and the second corresponds to the position of a particular mode when the frequencies for a specific wave number are arranged in ascending order. In the SSDQM results, ''a'' corresponds to anti-symmetric flexural mode and ''t'' to symmetric thickness mode. Therefore, $a=1$ and $t=1$ correspond to these modes for the first wave number and similarly so forth for their higher modes. It can be observed that for SS, GG and SG cases, rapid convergence with surprising numerical accuracy is observed for SSDQM results. The nature of convergence depends

Table 6. First 10 natural frequencies (Hz) of sandwich panels with SS, GG and SG edge boundary conditions.

f	1	2	3	4	5	6	7	8	9	10
SS_{SSM}	$622.56^{(1,1)}$	$1349.14^{(0,1)}$	$1526.56^{(2,1)}$	$2277.00^{(1,2)}$	$2432.37^{(2,2)}$	$2846.54^{(3,1)}$	$3264.15^{(3,2)}$	$4628.46^{(4,1)}$	$4825.01^{(4,2)}$	$6447.02^{(0,2)}$
SS_{SSDQM}	$622.56^{(a_1)}$	1349.14	$1526.56^{(a_2)}$	$2277.00^{(t_1)}$	$2432.37^{(t_2)}$	$2846.54^{(a_3)}$	$3264.15^{(t_3)}$	$4628.46^{(a_4)}$	$4825.01^{(t_4)}$	6447.02
SS_{FEM}	622.56	1349.1	1526.6	2277.0	2432.4	2846.5	3264.2	4628.5	4825.0	6447.0
GG_{SSM}	$622.56^{(1,1)}$	$1526.56^{(2,1)}$	$2277.00^{(1,2)}$	$2336.78^{(0,1)}$	$2432.37^{(2,2)}$	$2846.54^{(3,1)}$	$3264.15^{(3,2)}$	$4628.46^{(4,1)}$	$4825.01^{(4,2)}$	$6476.67^{(1,3)}$
GG_{SSDQM}	$622.56^{(a_1)}$	$1526.56^{(a_2)}$	$2277.00^{(t_1)}$	2336.78	$2432.37^{(t_2)}$	$2846.54^{(a_3)}$	$3264.15^{(t_3)}$	$4628.46^{(a_4)}$	$4825.01^{(t_4)}$	6476.67
GG_{FEM}	622.56	1526.6	2277.0	2336.8	2432.4	2846.5	3264.2	4628.5	4825.0	6476.67
SG_{SSM}	$283.17^{(1,1)}$	$1028.80^{(2,1)}$	$2129.97^{(3,1)}$	$2292.25^{(2,2)}$	$2312.09^{(1,2)}$	$2750.70^{(3,2)}$	$3679.37^{(4,1)}$	$3962.17^{(4,2)}$	$4289.09^{(1,3)}$	$4752.97^{(1,4)}$
SG_{SSDQM}	$283.17^{(a_1)}$	$1028.80^{(a_2)}$	$2129.97^{(a_3)}$	$2292.25^{(t_1)}$	$2312.09^{(t_2)}$	$2750.70^{(t_3)}$	$3679.37^{(a_4)}$	$3962.17^{(t_4)}$	4289.09	4752.97
SG_{FEM}	283.17	1028.8	2130.0	2292.2	2312.1	2750.7	3679.4	3962.2	4289.1	4753.0

Table 7. First 10 natural frequencies (Hz) of sandwich panels with different combinations of edge boundary conditions.

f	1	2	3	4	5	6	7	8	9	10
CC_{SSDQM}	$853.3^{(a_1)}$	$1998.1^{(a_2)}$	$2369.3^{(t_1)}$	$2793.3^{(t_2)}$	$3563.1^{(a_3)}$	$3958.0^{(t_3)}$	$5565.0^{(a_4)}$	$5759.8^{(t_4)}$	6489.9	7880.2
CC_{FEM}	853.37	1998.2	2369.3	2793.4	3563.3	3958.2	5565.4	5760.2	6489.9	7880.4
CF_{SSDQM}	$329.9^{(a_1)}$	$1092.4^{(a_2)}$	$2179.5^{(a_3)}$	$2276.3^{(t_1)}$	$2310.7^{(t_2)}$	$2783.6^{(t_3)}$	$3694.5^{(a_4)}$	$3944.9^{(t_4)}$	4304.5	4742.1
CF_{FEM}	329.88	1092.6	2179.2	2276.3	2310.8	2783.3	3695.2	3945.5	4304.0	4741.5
FF_{SSDQM}	$1303.0^{(a_1)}$	$1370.7^{(a_2)}$	$2246.1^{(t_1)}$	$2264.9^{(t_2)}$	$2310.2^{(t_3)}$	$2371.4^{(a_3)}$	$2758.8^{(t_4)}$	$3827.1^{(a_4)}$	$3965.0^{(t_5)}$	$5754.0^{(t_6)}$
FF_{FEM}	1303.0	1370.7	2246.1	2264.9	2310.2	2371.4	2758.8	3827.1	3965.0	5754.0
CS_{SSDQM}	$723.5^{(a_1)}$	$1746.2^{(a_2)}$	$2302.0^{(t_1)}$	$2597.0^{(t_2)}$	$3189.8^{(a_3)}$	$3594.5^{(t_3)}$	4290.1	4755.4	$5085.3^{(a_4)}$	$5289.0^{(t_4)}$
CS_{FEM}	723.53	1746.3	2302.0	2597.0	3189.9	3594.5	4290.1	4755.4	5085.5	5289.2
SF_{SSDQM}	$885.5^{(a_1)}$	$1375.2^{(a_2)}$	$1954.1^{(a_3)}$	$2257.4^{(t_1)}$	$2282.0^{(t_2)}$	$2571.8^{(t_3)}$	$3333.4^{(a_4)}$	$3594.9^{(t_4)}$	$5203.4^{(a_5)}$	$5293.6^{(t_5)}$
SF_{FEM}	885.54	1375.2	1954.1	2257.4	2282.0	2571.8	3333.4	3594.9	5203.4	5293.6
CG_{SSDQM}	$339.7^{(a_1)}$	$1187.5^{(a_2)}$	$2311.5^{(t_1)}$	$2382.3^{(t_2)}$	$2412.1^{(a_3)}$	$3001.1^{(t_3)}$	$4081.4^{(a_4)}$	$4364.3^{(t_4)}$	$6197.8^{(a_5)}$	$6325.4^{(t_5)}$
CG_{FEM}	339.68	1187.5	2311.4	2382.3	2412.1	3001.1	4081.5	4364.4	6198.1	6325.6
FG_{SSDQM}	$589.1^{(a_1)}$	$1399.7^{(a_2)}$	$2256.8^{(t_1)}$	$2307.2^{(t_2)}$	$2347.1^{(t_3)}$	$2572.3^{(a_3)}$	$2988.0^{(t_4)}$	$4204.8^{(a_4)}$	4261.5	$4400.7^{(t_5)}$
FG_{FEM}	589.09	1399.7	2256.8	2307.2	2347.1	2572.3	2988.0	4204.8	4261.5	4400.7

on the wave number of the frequency in which the structure vibrates. All modes specific to a particular wave number have the same nature of convergence. More grid points are required to obtain converged solutions for frequencies corresponding to higher wave numbers.

The convergence of SSDQM for cases which have no exact solutions is studied in Table 4. These values are compared with the results from FEM simulations. Unlike SSM, the wave number "m" does not appear in the SSDQM formulation and thus the frequencies specific to a particular wave number cannot be separated out. The positive real numbers that satisfy the frequency equation (21) are the

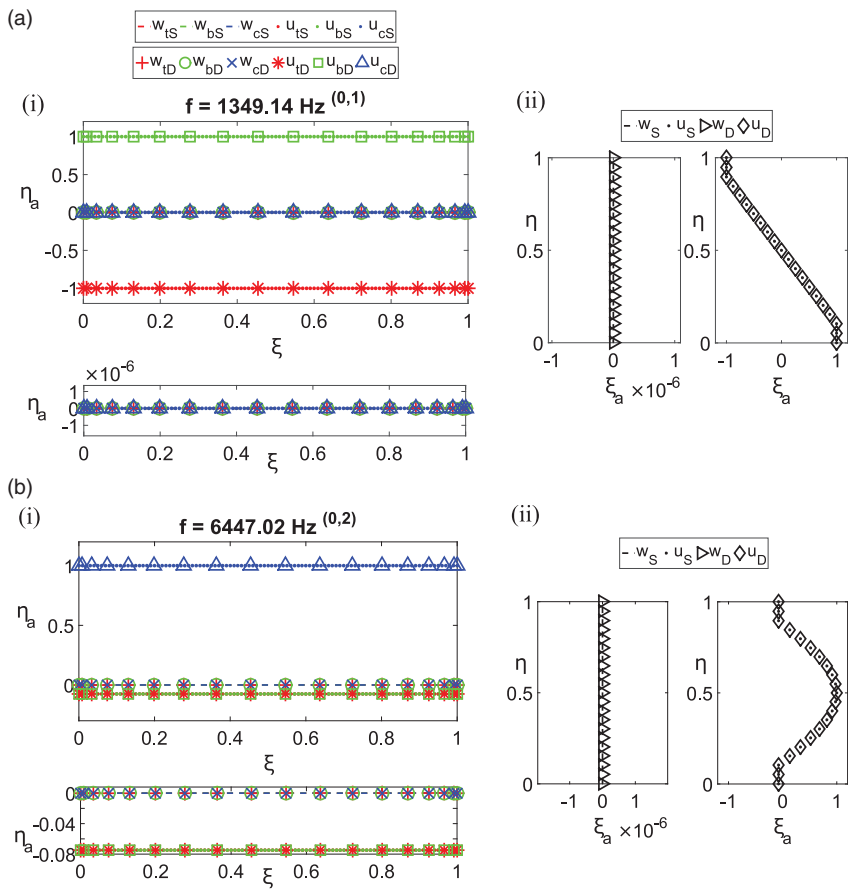

Figure 2. The first two displacement modes of SS panel for wave number $m = 0$. (a) First mode (0,1): (i) the longitudinal displacement modes; (ii) through-the-thickness displacement modes of u and w plotted, respectively, at cross-sections $\xi = 1$ and $\xi = 0.5$. (b) Second mode (0,2): (i) the longitudinal displacement modes; (ii) through-the-thickness displacement modes of u and w plotted, respectively, at cross-sections $\xi = 0.5$ and $\xi = 1$.

natural frequencies of the panel. The mode shapes, for all the frequencies listed in Tables 3 to 7, are plotted before classifying them as antisymmetric or symmetric type. Similar trends in convergence (as in Table 3) can be observed in Table 4. It can be noticed that the convergence of numerical results depend on the type of edge boundary condition. The rate of convergence in all these cases is slower than for the SS, GG and SG conditions, that is, more number of grid points are required for convergence. Also, convergence in cases including clamped edges are slower than that of the others. In practical applications, convergence up to the last integer place is more than sufficient. Therefore, SSDQM with $N = 17$ or $N = 19$ can give numerically accurate results for thick soft-core sandwich panels with any arbitrary edge boundary conditions.

Comparison with conventional SSDQM for CF panels

A comparison of numerical results, between the conventional (referred as CON) and modified (MOD) SSDQM for CF case, along with convergence studies, is given in Table 5. Here in obtaining 'CON' results, the conventional procedure followed in implementing the edge boundary condition for CF case (refer Appendix A [33]) is used along with the assembling procedure (of local transfer matrices) to form the global transfer matrix, so that the numerical errors due to multiplication of local transfer matrices are avoided, and therefore its comparison with the present results (MOD) would be on an equal footing. These are also compared with results from finite element simulation. From the study, it can clearly be understood that, compared to the conventional methodology, the modified

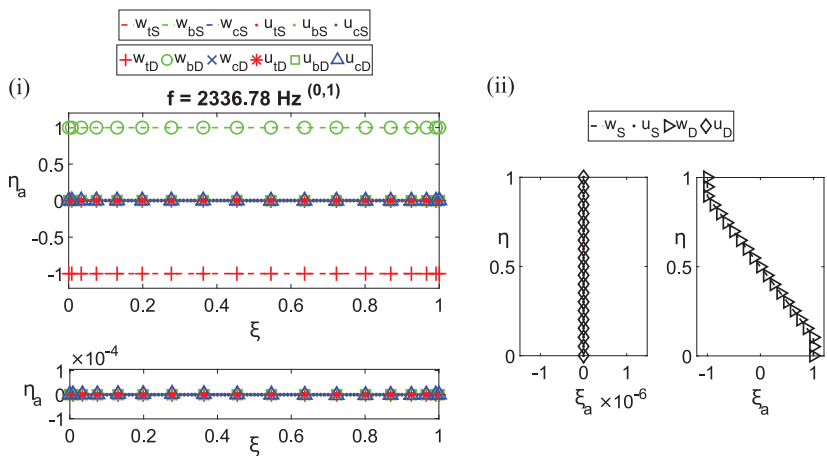

Figure 3. The first displacement mode (0,1) of GG panel for wave number $m = 0$: (i) the longitudinal displacement modes; (ii) through-the-thickness displacement modes of u and w plotted, respectively, at cross-sections $\xi = 0.5$ and $\xi = 1$.

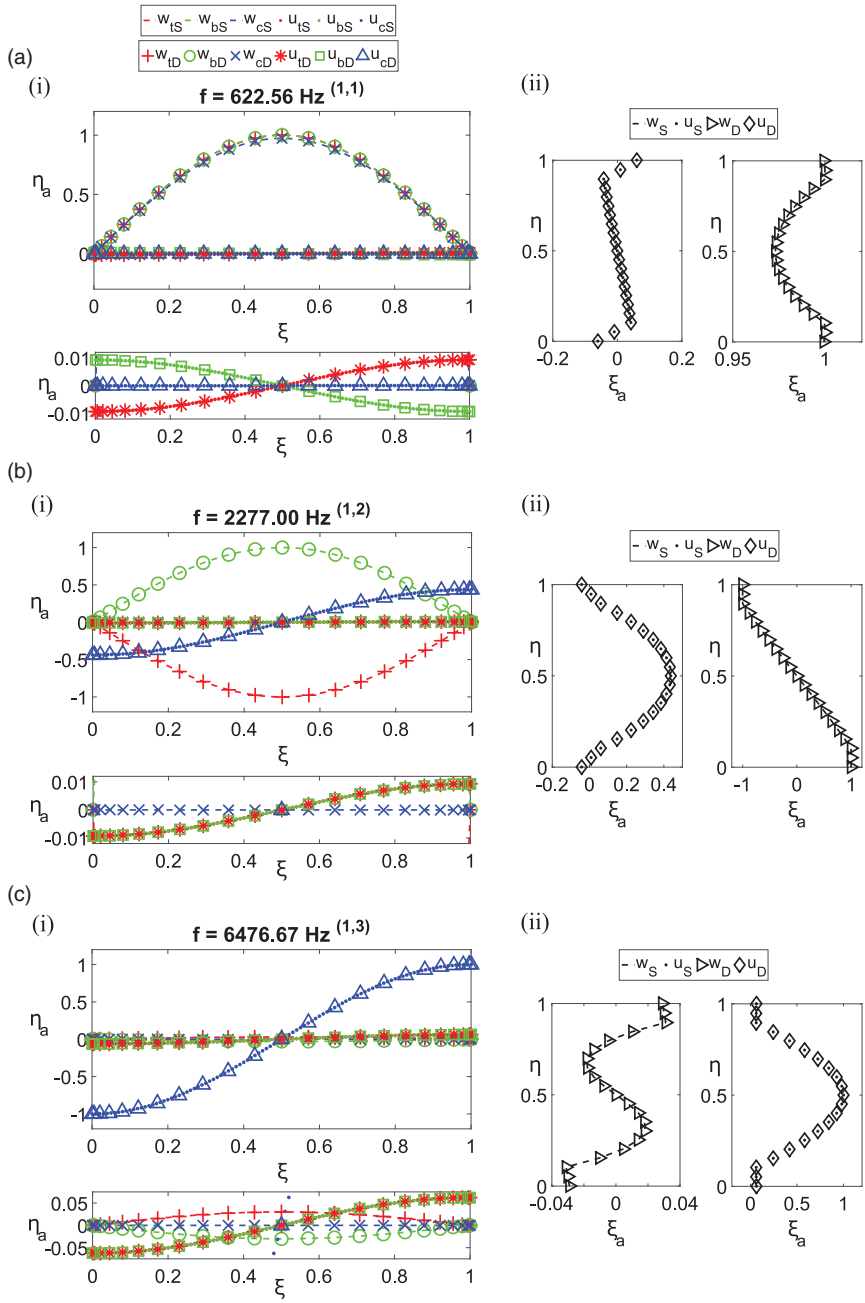

Figure 4. The first three displacement modes of SS panel for wave number $m = 1$. In the first (1,1), second (1,2) and third modes (1,3) ((a), (b) and (c) respectively): (i) the longitudinal displacement modes; (ii) through-the-thickness modes of u and w plotted, respectively, at cross-sections $\xi = 1$ and $\xi = 0.5$.

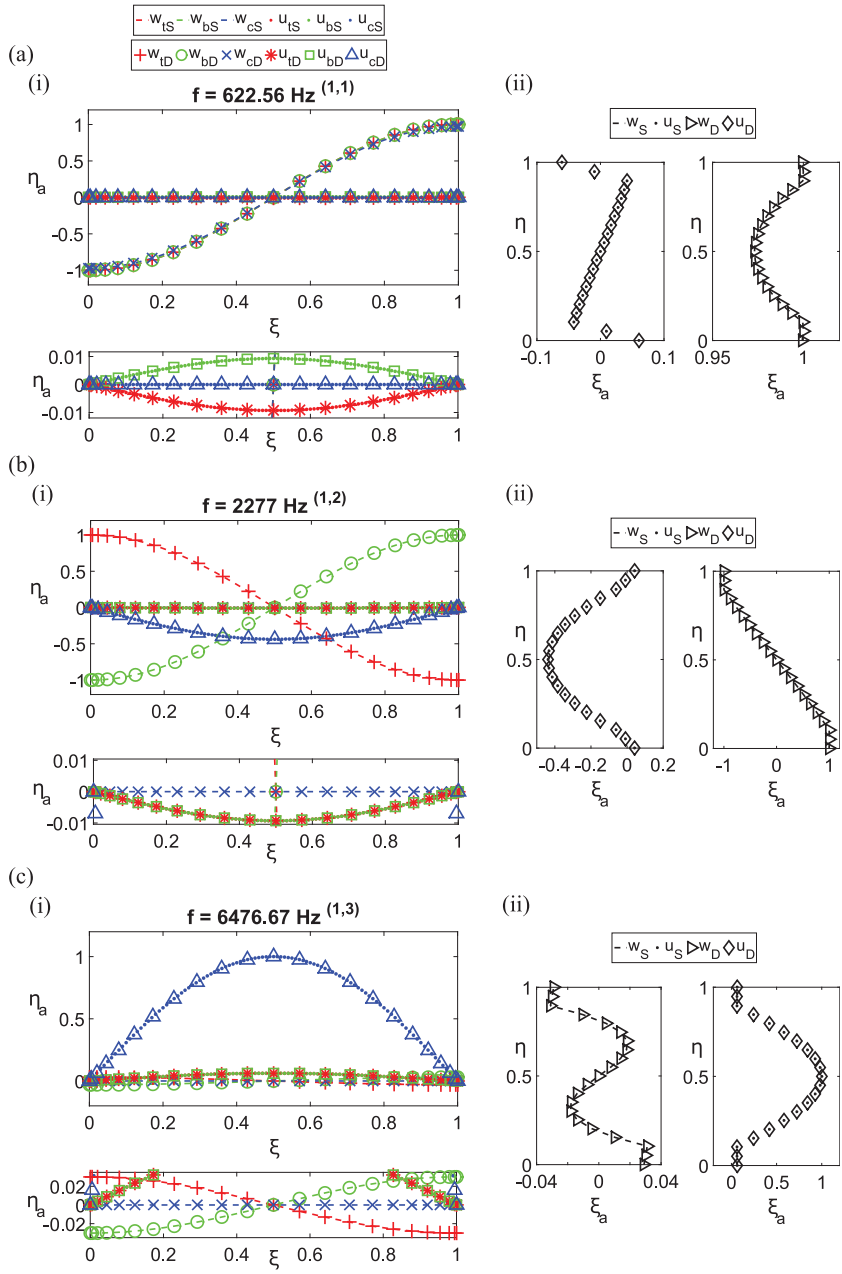

Figure 5. The first three displacement modes of GG panel for wave number $m = 1$. In the first (1,1), second (1,2) and third modes (1,3) ((a), (b) and (c) respectively): (i) the longitudinal displacement modes; (ii) through-the-thickness displacement modes of u and w plotted, respectively, at cross-sections $\xi = 0.5$ and $\xi = 1$.

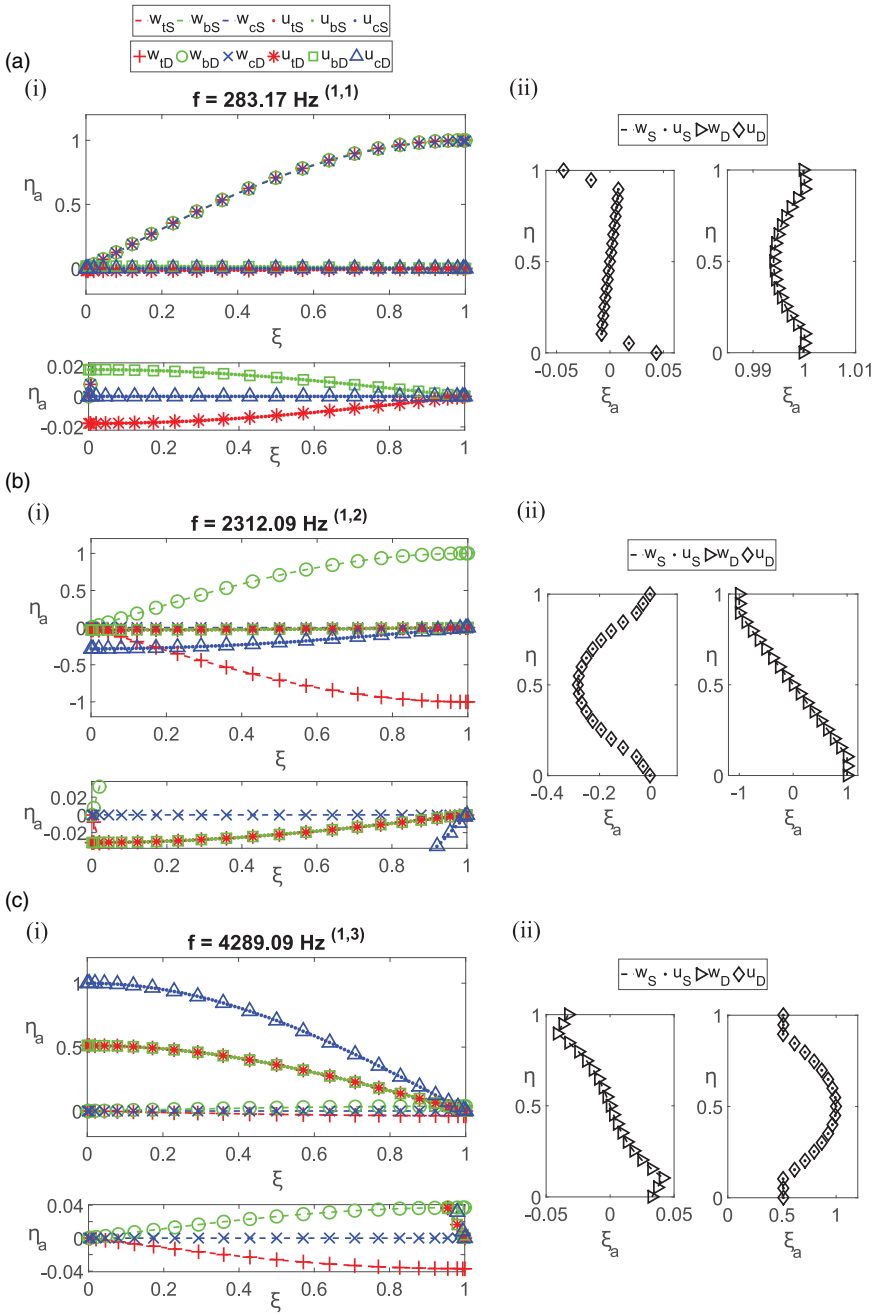

Figure 6. The first three displacement modes of SG panel for wave number $m = 1$. In the first (1,1), second (1,2) and third modes (1,3) ((a), (b) and (c) respectively): (i) the longitudinal displacement modes; (ii) through-the-thickness displacement modes of u and w plotted, respectively, at cross-sections $\xi = 0$ and $\xi = 1$.

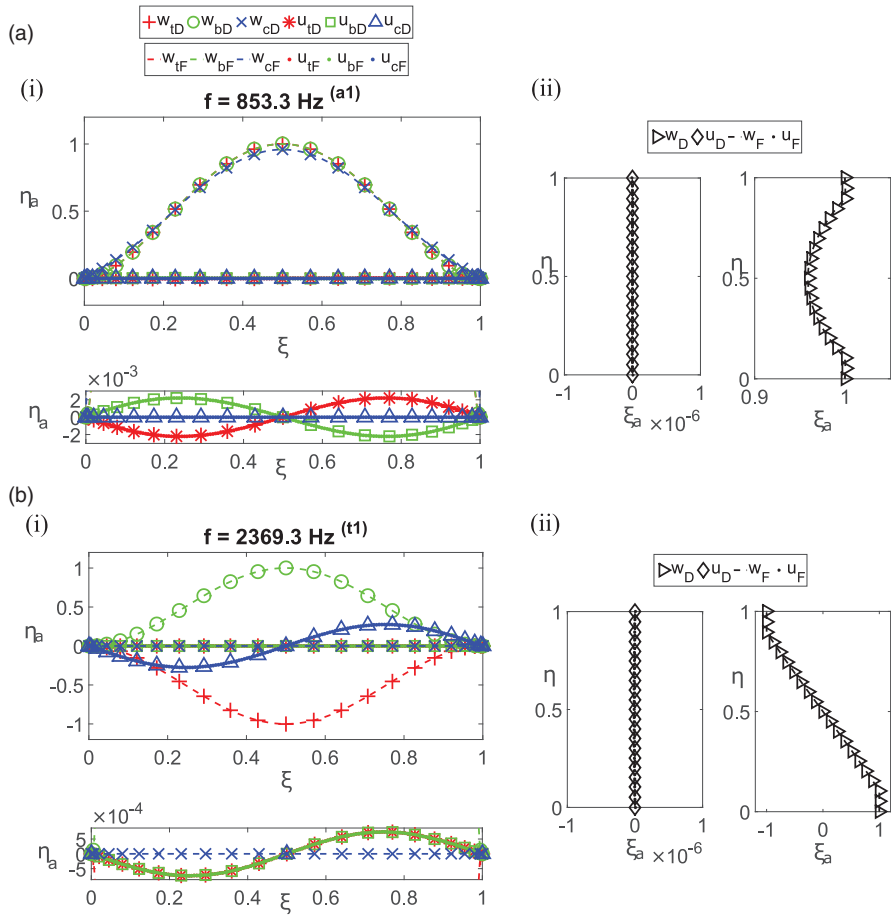

Figure 7. (a) The first anti-symmetric and (b) symmetric displacement modes of CC panel. In sub-figures (a) and (b): (i) the longitudinal displacement modes; (ii) through-the-thickness displacement modes of u and w plotted at cross-section $\xi = 0.5$.

formulation successfully predicts the natural frequencies (even for higher modes) with excellent numerical accuracy and convergence for thick, soft-core sandwich panels with CF condition.

Frequencies and mode shapes using modified SSDQM

Comparison of modified SSDQM with SSM. The first 10 natural frequencies for SS, GG and SG cases after satisfying proper convergence criteria are displayed in Table 6. An excellent match between the results of SSM and SSDQM is observed in all the cases. Along with these results, the natural frequencies from finite element analysis

are also presented. The results for the SS panel include frequencies (0,1),(0,2), corresponding to the in-plane modes of the zeroth wave number; (1,1),(2,1),...(4,1), the flexural antisymmetric modes of wave numbers 1,2,...,4 and frequencies (1,2),(2,2),...(4,2), the transverse symmetric (thickness) modes. There are other higher modes that include in-plane modes in which the core alone deforms $((1,3),(2,3),(3,3))$, in-plane deformation modes including both the core and the face sheets $((1,4),(1,5))$, other modes with combination of in-plane and transverse deformations in the core $((1,4),(1,5))$ all of which are not displayed. Most of the higher modes similar to these types are not presented for the

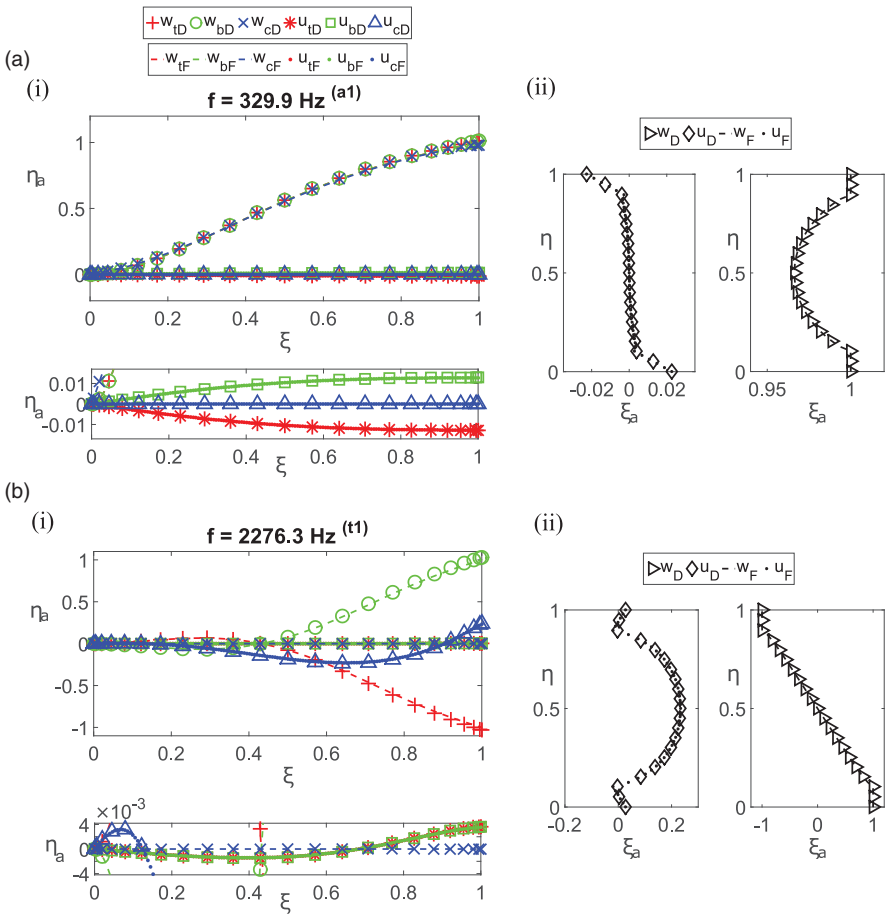

Figure 8. (a) The first anti-symmetric and (b) symmetric displacement modes of CF panel. In sub-figures (a) and (b): (i) the longitudinal displacement modes; (ii) through-the-thickness displacement modes of u and w plotted at cross-section $\xi = 1$.

different cases studied here. Similarly, natural frequencies are listed and classified for GG and SG cases.

When $m = 0$, for the SS case, the first two modes ((0,1) and (0,2)) obtained have frequencies 1349.14 Hz and 6447.02 Hz, and for GG case, the first mode (0,1) is 2336.78 Hz. The normalized mode shapes corresponding to these frequencies obtained using SSM and SSDQM are compared for SS and GG cases, respectively, in Figures 2 and 3. Similarly, the first three modes corresponding to $m = 1$ ((1,1),(1,2),(1,3)) for SS, GG and SG cases obtained using SSM and SSDQM are plotted in Figures 4 to 6.

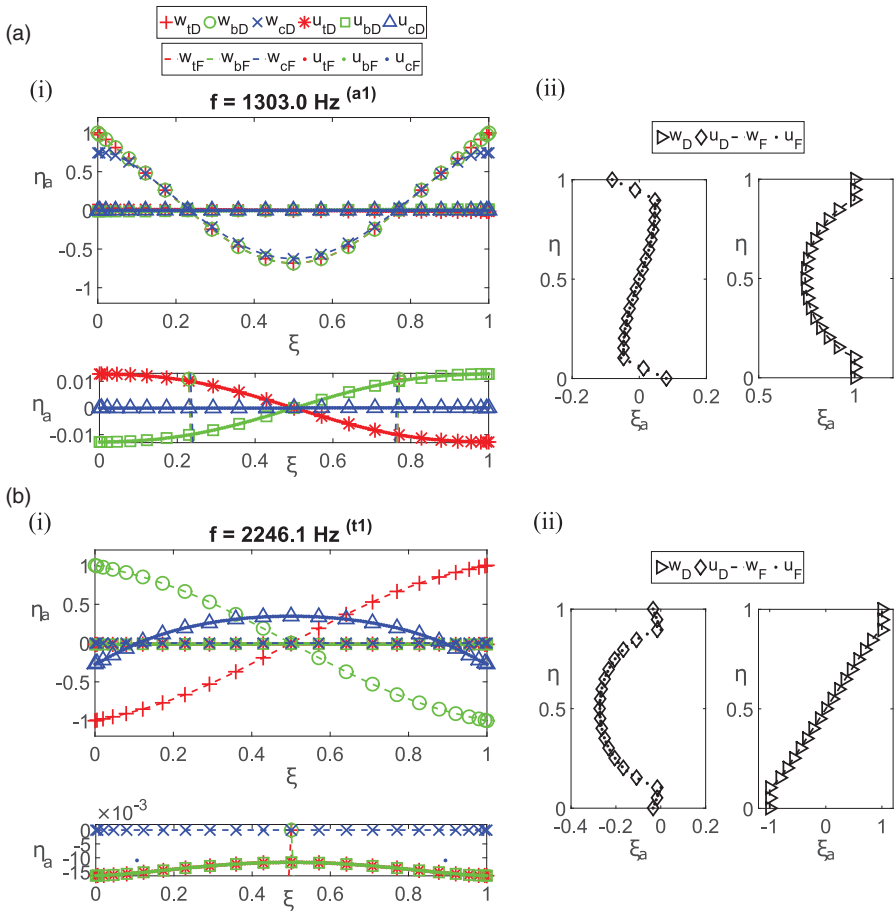

Figure 9. (a) The first anti-symmetric and (b) symmetric displacement modes of FF panel. In sub-figures (a) and (b): (i) the longitudinal displacement modes; (ii) through-the-thickness displacement modes of u and w plotted at cross-section $\xi = 1$.

Referring to the first plot (i.e. plot number (i)) within each of the sub-figures in Figures 2 to 6, the variables $\mathbf{w_{tS}}, \mathbf{w_{bS}}, \mathbf{w_{cS}}$ and $\mathbf{u_{tS}}, \mathbf{u_{bS}}, \mathbf{u_{cS}}$ correspond to the longitudinal displacement modes of transverse and in-plane displacements at mid-plane of the top face sheet, the bottom face sheet and the core obtained using SSM. Similarly, $\mathbf{w_{tD}}, \mathbf{w_{bD}}, \mathbf{w_{cD}}$ and $\mathbf{u_{tD}}, \mathbf{u_{bD}}, \mathbf{u_{cD}}$ correspond to those obtained using SSDQM. All these are the eigenmodes along the length of the panel and are normalized with respect to the largest value of displacement among them – separately done for SSM and SSDQM. A zoomed image is included in plot (i) of all sub-figures to better visualize the trends of variables with lower magnitude. In the second plot (i.e. plot number (ii)) within each of the sub-figures,

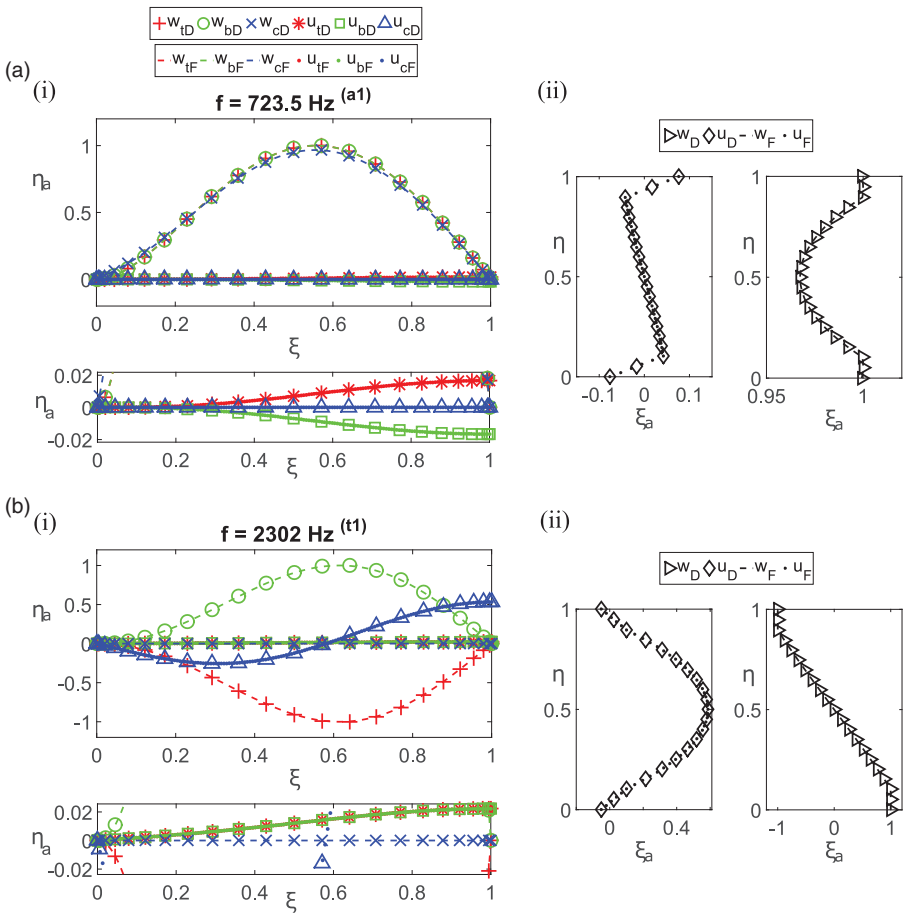

Figure 10. (a) The first anti-symmetric and (b) symmetric displacement modes of CS panel. In sub-figures (a) and (b): (i) the longitudinal displacement modes; (ii) through-the-thickness displacement modes of u and w plotted at $\xi = 0.5$.

$\mathbf{u_S}, \mathbf{u_D}$ and $\mathbf{w_S}, \mathbf{w_D}$ represent, respectively, the through-the-thickness modes of the in-plane and the transverse displacements normalized with respect to the largest value among them; separately for SSM and SSDQM. Zoomed plots of these variables are given separately so that even the minor trends in their distribution could, immediately, be identified. It should be noted that in plot (i) and (ii) of all these sub-figures, η_a and ξ_a denotes, respectively, the amplitude of longitudinal modes and through-the-thickness modes and these should not be confused with the respective normalized coordinates η and ξ. The through-the-thickness modes of transverse and in-plane displacements are plotted, respectively, at the mid-section ($\xi = 0.5$) and edge section ($\xi = 1$) of the panel for SS case and vice versa for GG case, whereas for SG panel, the edge sections $\xi = 0$ and $\xi = 1$ are, respectively, used for plotting in-plane and transverse displacements.

It is interesting to note that the numerical values of SS and GG cases are matching in all the cases (except for $m = 0$), even when their mode shapes

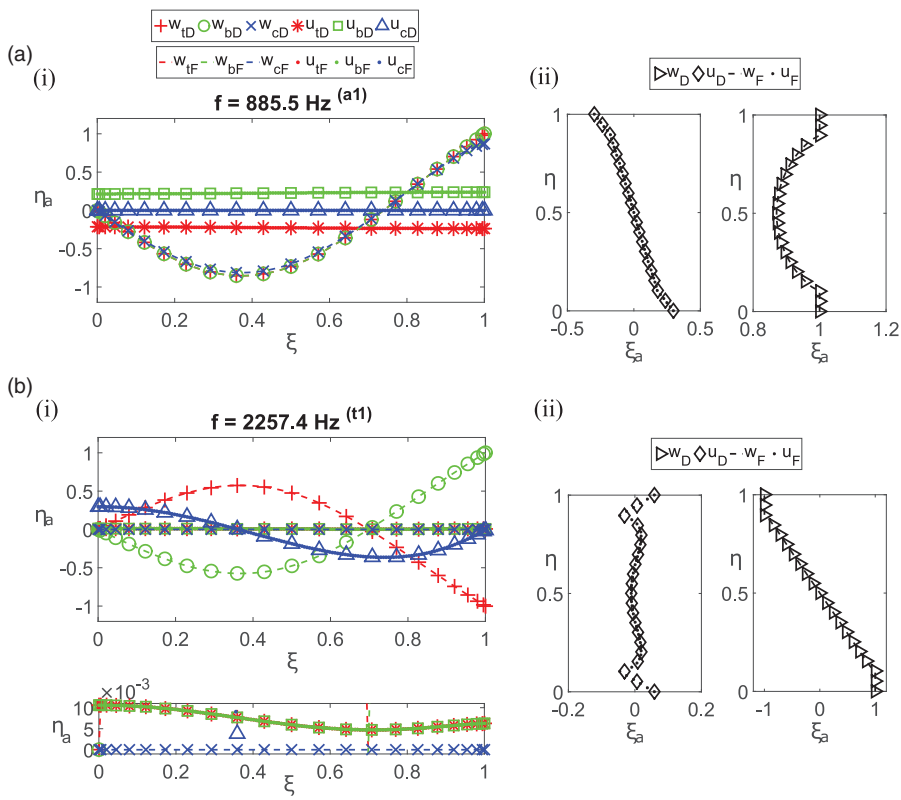

Figure 11. (a) The first anti-symmetric and (b) symmetric displacement modes of SF panel. In sub-figures (a) and (b): (i) the longitudinal displacement modes; (ii) through-the-thickness displacement modes of u and w plotted at cross-section $\xi = 1$.

drastically vary (see Table 6 and Figures 4 and 5). This can easily be reasoned out from the fact that both these cases have the same sub-matrix in the frequency equation (13). Another interesting observation is that unlike the SS and GG cases, the first and second symmetric modes ($t = 1$ and $t = 2$) for SG panel correspond to $m = 2$ and 1, respectively (see Figure 3 (for convergence of SG) and Figure 6 for details).

Comparison of modified SSDQM with FEM. The first 10 natural frequencies for cases without exact solutions are displayed in Table 7 along with FEM results for comparison. The SSDQM results given in Table 7 are for $N = 23$, after rounding off to the first decimal place. The SSDQM and FEM results match very well for all cases.

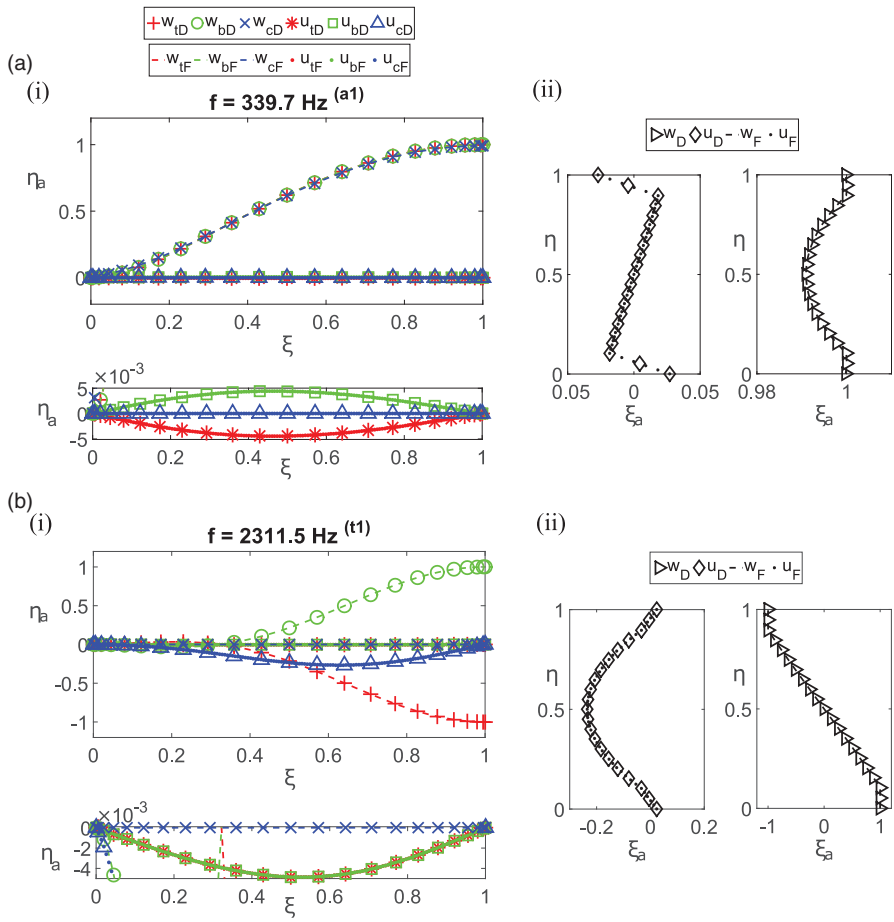

Figure 12. (a) The first anti-symmetric and (b) symmetric displacement modes of CG panel. In sub-figures (a) and (b): (i) the longitudinal displacement modes; (ii) through-the-thickness displacement modes of u and w plotted, respectively, at cross-sections $\xi = 0.5$ and $\xi = 1$.

The mode shapes of these panels obtained using SSDQM and FEM simulations are displayed from Figures 7 to 13. In plot (i), within each sub-figures, $\mathbf{w_{tD}, w_{bD}, w_{cD}, u_{tD}, u_{bD}, u_{cD}}$ and $\mathbf{w_{tF}, w_{bF}, w_{cF}, u_{tF}, u_{bF}, u_{cF}}$ correspond, respectively, to the SSDQM and FEM solutions. These are the longitudinal modes of in-plane and transverse displacements normalized with respect to the largest value among them (except for CS case where all variables are normalized with respect to maximum value of transverse displacement at mid-cross-section) – separately for SSDQM and FEM. In the second plot (i.e. plot number (ii)) within each of these sub-figures, $(\mathbf{w_D}, \mathbf{u_D})$ and $(\mathbf{w_F}, \mathbf{u_F})$ represent, respectively, the SSDQM and FEM solutions for through-the-thickness modes. The in-plane and the transverse

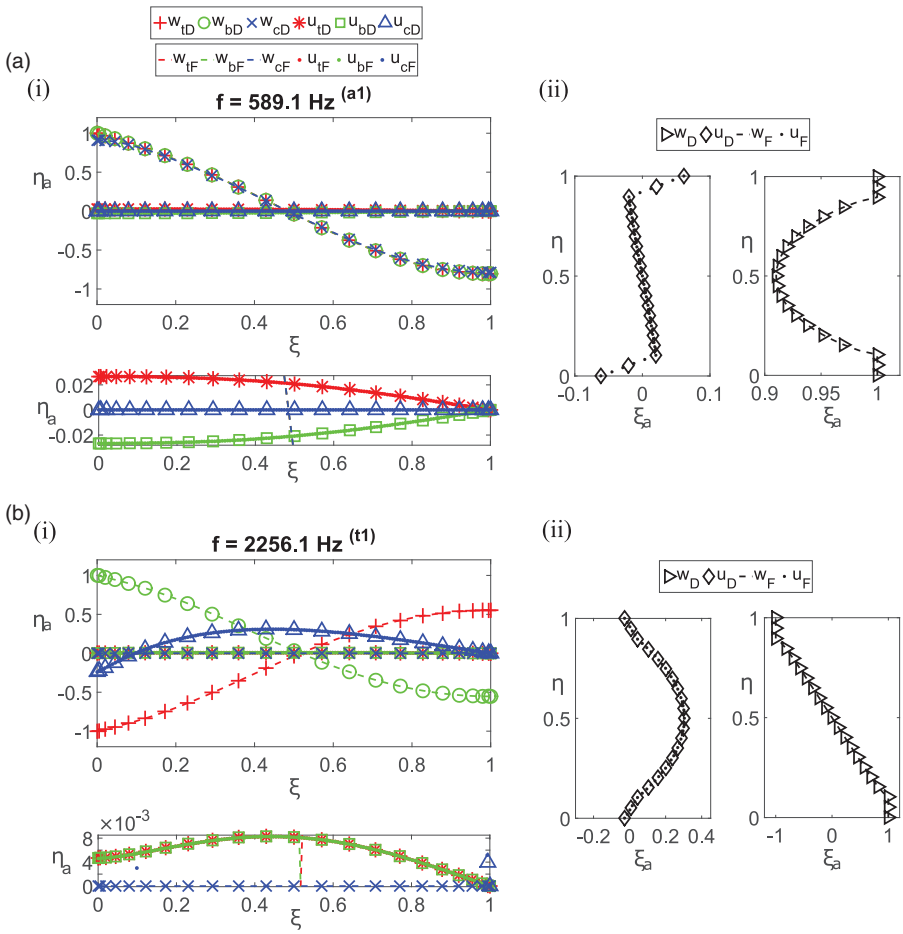

Figure 13. (a) The first anti-symmetric and (b) symmetric displacement modes of FG panel. In sub-figures (a) and (b): (i) the longitudinal displacement modes; (ii) through-the-thickness displacement modes of u and w plotted, respectively, at cross-sections $\xi = 0.5$ and $\xi = 0$.

displacements are normalized with respect to the largest value among them; separately for SSDQM and FEM. The mode shapes corresponding to the first antisymmetric mode ($a = 1$) and the first symmetric mode ($t = 1$) are presented in each case. For the CC and CS cases (see Figures 7 and 10), the mid section ($\xi = 0.5$) of the panel is considered for plotting the through-the-thickness transverse and in-plane displacement modes, whereas for CF, FF and SF edges (Figures 8, 9 and 11), these modes at the edge section $\xi = 1$ are displayed. In CG case (refer Figure 12), the mid-section is used for in-plane displacement and edge section $\xi = 1$ for transverse displacement. However, in FG case (see Figure 13), the mid-section is used for plotting the in-plane displacements and edge section $\xi = 0$ for transverse displacements. An excellent match between each solutions of SSDQM and FEM is observed in all the cases studied.

Conclusions

Based on the exact two-dimensional elasticity model, the natural frequencies and the mode shapes of thick, soft-core sandwich panels with different combinations of edge boundary conditions are presented. New exact elasticity solutions are obtained using the SSM for sandwich panels with combination of simply supported and guided. A systematic procedure is proposed to implement all combinations of edge boundary conditions, including simply supported, clamped, free and guided, in the SSDQM. The convergence and accuracy of the modified SSDQM is tested using exact elasticity solutions from SSM and approximate solutions from FEM simulations. The modified semi-analytical methodology is found to give numerically accurate solutions with rapid convergence for all the cases studied and for higher modes of vibration. The proposed modifications lead to a more general framework when compared to the conventional SSDQM formulation as it include all combinations of edge boundary conditions. Moreover, the present methodology is found to give results with better numerical accuracy and faster convergence compared to the conventional approach for thick, cantilevered sandwich panels. These results based on exact elasticity model can be referred as benchmarks for validating results from approximate models for arbitrary edge boundary conditions. As there are no approximations in the field variables, these results can also be used to develop and test new approximate models for soft-core sandwich panels with arbitrary edge boundary conditions.

Declaration of conflicting interests

The author(s) declared no potential conflicts of interest with respect to the research, authorship, and/or publication of this article.

Funding

The author(s) received no financial support for the research, authorship, and/or publication of this article.

References

1. Allen HG. *Analysis and design of structural sandwich panels*. Oxford: Pergamon, 1969.
2. Plantema FJ. *Sandwich construction,* volume 199631. New York: Wiley, 1966.
3. Vinson JR. *The behavior of sandwich structures of isotropic and composite materials*. Lancaster: Technomic Publishing CO.INC., CRC Press, 1999, 1999.
4. Burton WS and Noor AK. Assessment of computational models for sandwich panels and shells. *Comput Meth Appl Mech Eng* 1995; 124: 125–151.
5. Noor AK, Burton WS and Bert CW. Computational models for sandwich panels and shells. *Appl Mech Rev* 1996; 49: 155–199.
6. Frostig Y. Classical and high-order computational models in the analysis of modern sandwich panels. *Compos Part B: Eng* 2003; 34: 83–100.
7. Reddy JN. *Mechanics of laminated composite plates and shells: theory and analysis*. Boca Raton: CRC Press, 2004, 2004.
8. Carrera E and Brischetto S. A survey with numerical assessment of classical and refined theories for the analysis of sandwich plates. *Appl Mech Rev* 2009; 62: 010803-1–17.
9. Frostig Y and Baruch M. Bending of sandwich beams with transversely flexible core. *AIAA J* 1990; 28: 523–531.
10. Frostig Y and Baruch M. Free vibrations of sandwich beams with a transversely flexible core: a high order approach. *J Sound Vibr* 1994; 176: 195–208.
11. Frostig Y and Thomsen OT. High-order free vibration of sandwich panels with a flexible core. *Int J Solids Struct* 2004; 41: 1697–1724.
12. Phan CN, Frostig Y and Kardomateas GA. Analysis of sandwich beams with a compliant core and with in-plane rigidity – extended high-order sandwich panel theory versus elasticity. *J Appl Mech* 2012; 79: 041001-1–11.
13. Frostig Y, Phan CN and Kardomateas GA. Free vibration of unidirectional sandwich panels, part i: Compressible core. *J Sandw Struct Mater* 2013; 15: 377–411.
14. Phan CN, Frostig Y and Kardomateas GA. Free vibration of unidirectional sandwich panels, part ii: Incompressible core. *J Sandw Struct Mater* 2013; 15: 412–428.
15. Sokolinsky VS, Von Bremen HF, Lavoie JA, et al. Analytical and experimental study of free vibration response of soft-core sandwich beams. *J Sandw Struct Mater* 2004; 6: 239–261.
16. Wang Y and Wang X. Free vibration analysis of soft-core sandwich beams by the novel weak form quadrature element method. *J Sandw Struct Mater* 2015; 18: 294–320.
17. Pagano NJ. Exact solutions for composite laminates in cylindrical bending. *J Compos Mater* 1969; 3: 398–411.
18. Pagano NJ. Exact solutions for rectangular bidirectional composites and sandwich plates. *J Compos Mater* 1970; 4: 20–34.
19. Srinivas S and Rao AK. Bending, vibration and buckling of simply supported thick orthotropic rectangular plates and laminates. *Int J Solids Struct* 1970; 6: 1463–1481.
20. Zenkour AM. Three-dimensional elasticity solution for uniformly loaded cross-ply laminates and sandwich plates. *J Sandw Struct Mater* 2007; 9: 213–238.
21. Kardomateas GA. Three-dimensional elasticity solution for sandwich plates with orthotropic phases: the positive discriminant case. *J Appl Mech* 2009; 76: 014505-1–4.
22. Kardomateas GA and Phan CN. Three-dimensional elasticity solution for sandwich beams/wide plates with orthotropic phases: the negative discriminant case. *J Sandw Struct Mater* 2011; 13: 641–661.

23. Wu CP, Chiu KH and Wang YM. A review on the three-dimensional analytical approaches of multilayered and functionally graded piezoelectric plates and shells. *Comput Mater Continua* 2008; 8: 93–132.
24. Bahar LY. Transfer matrix approach to layered systems. *J Eng Mech Div* 1972; 98: 1159–1172.
25. Bahar LY. A state space approach to elasticity. *J Franklin Inst* 1975; 299: 33–41.
26. Jiarang F and Jianqiao Y. An exact solution for the statics and dynamics of laminated thick plates with orthotropic layers. *Int J Solids Struct* 1990; 26: 655–662.
27. Sheng H and Ye J. A state space finite element for laminated composite plates. *Comput Meth Appl Mech Eng* 2002; 191: 4259–4276.
28. Qing G, Qiu J and Liu Y. Free vibration analysis of stiffened laminated plates. *Int J Solids Struct* 2006; 43: 1357–1371.
29. Qing G, Qiu J and Liu Y. A semi-analytical solution for static and dynamic analysis of plates with piezoelectric patches. *Int J Solids Struct* 2006; 43: 1388–1403.
30. Ye J. *Laminated composite plates and shells: 3D modelling*. London: Springer, 2003.
31. Bert CW and Malik M. Differential quadrature method in computational mechanics: a review. *Appl Mech Rev* 1996; 49: 1–28.
32. Shu C. *Differential quadrature and its application in engineering*. London: Springer, 2000.
33. Chen WQ, Lv CF and Bian ZG. Elasticity solution for free vibration of laminated beams. *Compos Struct* 2003; 62: 75–82.
34. Chen WQ and Lee KY. On free vibration of cross-ply laminates in cylindrical bending. *J Sound Vibr* 2004; 273: 667–676.
35. Chen WQ and Lü CF. 3D free vibration analysis of cross-ply laminated plates with one pair of opposite edges simply supported. *Compos Struct* 2005; 69: 77–87.
36. Lü CF, Chen WQ and Shao JW. Semi-analytical three-dimensional elasticity solutions for generally laminated composite plates. *Eur J Mech – A/Solids* 2008; 27: 899–917.

Appendix 1

In all the following equations, C_{ij} and ρ vary with respect to different layers of the sandwich panel.

The state equations for any layer are as follows

$$\begin{aligned}
\frac{\partial \bar{u}}{\partial \eta} &= -\lambda \frac{\partial \bar{w}}{\partial \xi} + \frac{C_{55}^{(b)}}{C_{55}} \tau \\
\frac{\partial \sigma_\eta}{\partial \eta} &= -\frac{\rho}{\rho^{(b)}} \Omega^2 \bar{w} - \lambda \frac{\partial \tau}{\partial \xi} \\
\frac{\partial \bar{w}}{\partial \eta} &= -\frac{C_{13}}{C_{33}} \lambda \frac{\partial \bar{u}}{\partial \xi} + \frac{C_{55}^{(b)}}{C_{33}} \sigma_\eta \\
\frac{\partial \tau}{\partial \eta} &= -\mathrm{A}_{\mathrm{XX}} \lambda \frac{\partial^2 \bar{u}}{\partial \xi^2} - \frac{\rho}{\rho^{(b)}} \Omega^2 \bar{u} - \frac{C_{13}}{C_{33}} \lambda \frac{\partial \sigma_\eta}{\partial \xi}
\end{aligned} \tag{22}$$

The derived variable is given by

$$\sigma_\xi = \mathrm{A_{XX}} \frac{\partial \bar{u}}{\partial \xi} + \frac{C_{13}}{C_{33}} \sigma_\eta, \quad \mathrm{A_{XX}} = \left(C_{11} - \frac{C_{13}^2}{C_{33}} \right) \frac{\lambda}{C_{55}^{(b)}} \tag{23}$$

In $\mathrm{A_{XX}}$, XX = SS, GG, SG, CC, CF, FF, SF, CG, FG. The sub-matrices of the coefficient matrix for the governing state equations are

$$\mathbf{A} = \begin{bmatrix} -\lambda \partial_\xi & \frac{C_{55}^{(b)}}{C_{55}} \\ -\frac{\rho}{\rho^{(b)}} \Omega^2 & -\lambda \partial_\xi \end{bmatrix} \quad \mathbf{B} = \begin{bmatrix} -\frac{C_{13}}{C_{33}} \lambda \partial_\xi & \frac{C_{55}^{(b)}}{C_{33}} \\ -\mathrm{A_{XX}} \lambda \, \partial_\xi^2 - \frac{\rho}{\rho^{(b)}} \Omega^2 & -\frac{C_{13}}{C_{33}} \lambda \partial_\xi \end{bmatrix} \tag{24}$$

The sub-matrices of the coefficient matrix for the governing state equations for SS, GG and SG are as follows

$$\begin{aligned}
\overline{\mathbf{A}}_{\mathrm{SS}} &= \begin{bmatrix} -\lambda m\pi & \frac{C_{55}^{(b)}}{C_{55}} \\ -\frac{\rho}{\rho^{(b)}} \Omega^2 & \lambda m\pi \end{bmatrix} \quad \overline{\mathbf{B}}_{\mathrm{SS}} = \begin{bmatrix} \frac{C_{13}}{C_{33}} \lambda m\pi & \frac{C_{55}^{(b)}}{C_{33}} \\ \mathrm{A_{XX}} \lambda \, (m\pi)^2 - \frac{\rho}{\rho^{(b)}} \Omega^2 & -\frac{C_{13}}{C_{33}} \lambda m\pi \end{bmatrix} \\
\overline{\mathbf{A}}_{\mathrm{GG}} &= \begin{bmatrix} \lambda m\pi & \frac{C_{55}^{(b)}}{C_{55}} \\ -\frac{\rho}{\rho^{(b)}} \Omega^2 & -\lambda m\pi \end{bmatrix} \quad \overline{\mathbf{B}}_{\mathrm{GG}} = \begin{bmatrix} -\frac{C_{13}}{C_{33}} \lambda m\pi & \frac{C_{55}^{(b)}}{C_{33}} \\ \mathrm{A_{XX}} \lambda \, (m\pi)^2 - \frac{\rho}{\rho^{(b)}} \Omega^2 & \frac{C_{13}}{C_{33}} \lambda m\pi \end{bmatrix} \\
\overline{\mathbf{A}}_{\mathrm{SG}} &= \begin{bmatrix} -(2m-1)\lambda \frac{\pi}{2} & \frac{C_{55}^{(b)}}{C_{55}} \\ -\frac{\rho}{\rho^{(b)}} \Omega^2 & (2m-1)\lambda \frac{\pi}{2} \end{bmatrix} \\
\overline{\mathbf{B}}_{\mathrm{SG}} &= \begin{bmatrix} \frac{C_{13}}{C_{33}} (2m-1)\lambda \frac{\pi}{2} & \frac{C_{55}^{(b)}}{C_{33}} \\ \mathrm{A_{XX}} \lambda \left((2m-1) \frac{\pi}{2} \right)^2 - \frac{\rho}{\rho^{(b)}} \Omega^2 & -\frac{C_{13}}{C_{33}} (2m-1)\lambda \frac{\pi}{2} \end{bmatrix}
\end{aligned} \tag{25}$$

The sub-matrices of the coefficient matrix for the discretized state equations in matrix form

$$\mathbf{E} = \begin{bmatrix} -\lambda \mathbf{X}^{(1)} & \frac{C_{55}^{(b)}}{C_{55}} \mathbf{I} \\ -\frac{\rho}{\rho^{(b)}} \Omega^2 \mathbf{I} & -\lambda \mathbf{X}^{(1)} \end{bmatrix} \quad \mathbf{F} = \begin{bmatrix} -\frac{C_{13}}{C_{33}} \lambda \mathbf{X}^{(1)} & \frac{C_{55}^{(b)}}{C_{33}} \mathbf{I} \\ -\mathrm{A_{XX}} \lambda \, \mathbf{X}^{(2)} - \frac{\rho}{\rho^{(b)}} \Omega^2 \mathbf{I} & -\frac{C_{13}}{C_{33}} \lambda \mathbf{X}^{(1)} \end{bmatrix} \tag{26}$$

State equations at any grid point are separately listed below

$$\frac{d\bar{u}_i}{d\eta} = -\lambda \sum_{j=1}^{N} X_{ij}^{(1)} \bar{w}_j + \frac{C_{55}^{(b)}}{C_{55}} \tau_i$$

$$\frac{d\sigma_{\eta i}}{d\eta} = -\frac{\rho}{\rho^{(b)}} \Omega^2 \bar{w}_i - \lambda \sum_{j=1}^{N} X_{ij}^{(1)} \tau_j$$

$$\frac{d\bar{w}_i}{d\eta} = -\frac{C_{13}}{C_{33}}\lambda \sum_{j=1}^{N} X_{ij}^{(1)}\bar{u}_j + \frac{C_{55}^{(b)}}{C_{33}}\sigma_{\eta i}$$
$$\frac{d\tau_i}{d\eta} = -A_{\mathrm{XX}}\lambda \sum_{j=1}^{N} X_{ij}^{(2)}\bar{u}_j - \frac{\rho}{\rho^{(b)}}\Omega^2\bar{u}_i - \frac{C_{13}}{C_{33}}\lambda \sum_{j=1}^{N} X_{ij}^{(1)}\sigma_{\eta j} \tag{27}$$

The derived variable at any grid point is given by the following equation

$$\sigma_{\xi i} = \mathrm{A}_{\mathrm{XX}} \sum_{j=1}^{N} X_{ij}^{(1)}\bar{u}_j + \frac{C_{13}}{C_{33}}\sigma_{\eta i}, \quad i = 1, 2, \ldots, N \tag{28}$$

Equations after implementing different edge boundary conditions:

- Simply supported-simply supported (SS)

$$\frac{d\bar{u}_i}{d\eta} = -\lambda \sum_{j=2}^{N-1} X_{ij}^{(1)}\bar{w}_j + \frac{C_{55}^{(b)}}{C_{55}}\tau_i, \quad i = 1, 2, \ldots, N$$
$$\frac{d\sigma_{\eta i}}{d\eta} = -\frac{\rho}{\rho^{(b)}}\Omega^2\bar{w}_i - \lambda \sum_{j=1}^{N} X_{ij}^{(1)}\tau_j, \quad i = 2, ..., N-1$$
$$\frac{d\bar{w}_i}{d\eta} = -\frac{C_{13}}{C_{33}}\lambda \sum_{j=1}^{N} X_{ij}^{(1)}\bar{u}_j + \frac{C_{55}^{(b)}}{C_{33}}\sigma_{\eta i}, \quad i = 2, ..., N-1 \tag{29}$$
$$\frac{d\tau_i}{d\eta} = A_{\mathrm{SS}}\lambda \sum_{j=1}^{N} \left(X_{i1}^{(1)}X_{1j}^{(1)} + X_{iN}^{(1)}X_{Nj}^{(1)} - X_{ij}^{(2)}\right)\bar{u}_j - \frac{\rho}{\rho^{(b)}}\Omega^2\bar{u}_i$$
$$- \frac{C_{13}}{C_{33}}\lambda \sum_{j=2}^{N-1} X_{ij}^{(1)}\sigma_{\eta j}, \quad i = 1, 2, \ldots, N$$

- Guided-Guided (GG)

$$\frac{d\bar{u}_i}{\mathrm{d}\eta} = -\lambda \sum_{j=1}^{N} X_{ij}^{(1)}\bar{w}_j + \frac{C_{55}^{(b)}}{C_{55}}\tau_i, \quad i = 2, \ldots, N-1$$
$$\frac{d\sigma_{\eta i}}{\mathrm{d}\eta} = -\frac{\rho}{\rho^{(b)}}\Omega^2\bar{w}_i - \lambda \sum_{j=2}^{N-1} X_{ij}^{(1)}\tau_j, \quad i = 1, 2, \ldots, N \tag{30}$$

$$\frac{d\bar{w}_i}{\mathrm{d}\eta} = -\frac{C_{13}}{C_{33}}\lambda \sum_{j=2}^{N-1} X_{ij}^{(1)}\bar{u}_j + \frac{C_{55}^{(b)}}{C_{33}}\sigma_{\eta i}, \quad i = 1, 2, \ldots, N$$

$$\frac{d\tau_i}{\mathrm{d}\eta} = -\mathrm{A_{GG}}\lambda \sum_{j=2}^{N-1} X_{ij}^{(2)}\bar{u}_j - \frac{\rho}{\rho^{(b)}}\Omega^2\bar{u}_i - \frac{C_{13}}{C_{33}}\lambda \sum_{j=1}^{N} X_{ij}^{(1)}\sigma_{\eta j}, \quad i = 2, \ldots, N-1$$

- Simply supported-Guided (SG)

$$\begin{aligned}
\tfrac{d\bar{u}_i}{\mathrm{d}\eta} = &\quad -\lambda \sum_{j=2}^{N} X_{ij}^{(1)}\bar{w}_j + \tfrac{C_{55}^{(b)}}{C_{55}}\tau_i, \quad i = 1, 2, \ldots, N-1 \\
\tfrac{d\sigma_{\eta i}}{\mathrm{d}\eta} = &\quad -\tfrac{\rho}{\rho^{(b)}}\Omega^2\bar{w}_i - \lambda \sum_{j=1}^{N-1} X_{ij}^{(1)}\tau_j, \quad i = 2, \ldots, N \\
\tfrac{d\bar{w}_i}{\mathrm{d}\eta} = &\quad -\tfrac{C_{13}}{C_{33}}\lambda \sum_{j=1}^{N-1} X_{ij}^{(1)}\bar{u}_j + \tfrac{C_{55}^{(b)}}{C_{33}}\sigma_{\eta i}, \quad i = 2, \ldots, N \\
\tfrac{d\tau_i}{\mathrm{d}\eta} = &\quad -\mathrm{A_{SG}}\lambda \sum_{j=1}^{N-1} \left(X_{ij}^{(2)} + X_{i1}^{(1)}X_{1j}^{(1)}\right)\bar{u}_j - \tfrac{\rho}{\rho^{(b)}}\Omega^2\bar{u}_i \\
&\quad -\tfrac{C_{13}}{C_{33}}\lambda \sum_{j=2}^{N} X_{ij}^{(1)}\sigma_{\eta j}, \quad i = 1, 2, \ldots, N-1
\end{aligned} \tag{31}$$

- Clamped-Clamped (CC)

$$\begin{aligned}
\tfrac{d\bar{u}_i}{\mathrm{d}\eta} = &\quad -\lambda \sum_{j=2}^{N-1} X_{ij}^{(1)}\bar{w}_j + \tfrac{C_{55}^{(b)}}{C_{55}}\tau_i, \; i = 2, \ldots, N-1 \\
\tfrac{d\sigma_{\eta i}}{\mathrm{d}\eta} = &\quad -\tfrac{\rho}{\rho^{(b)}}\Omega^2\bar{w}_i + \tfrac{C_{55}}{C_{55}^{(b)}}\lambda^2 \sum_{j=2}^{N-1} \left(X_{i1}^{(1)}X_{1j}^{(1)} + X_{iN}^{(1)}X_{Nj}^{(1)}\right)\bar{w}_j \\
&\quad -\lambda \sum_{j=2}^{N-1} X_{ij}^{(1)}\tau_j, \; i = 2, \ldots, N-1 \\
\tfrac{d\bar{w}_i}{\mathrm{d}\eta} = &\quad -\tfrac{C_{13}}{C_{33}}\lambda \sum_{j=2}^{N-1} X_{ij}^{(1)}\bar{u}_j + \tfrac{C_{55}^{(b)}}{C_{33}}\sigma_{\eta i}, \; i = 2, \ldots, N-1 \\
\tfrac{d\tau_i}{\mathrm{d}\eta} = &\quad -\mathrm{A_{CC}}\lambda \sum_{j=2}^{N-1} X_{ij}^{(2)}\bar{u}_j - \tfrac{\rho}{\rho^{(b)}}\Omega^2\bar{u}_i \\
&\quad -\left(\tfrac{C_{13}^2}{C_{33}}\tfrac{\lambda^2}{C_{55}^{(b)}}\right) \sum_{j=2}^{N-1} \left(X_{i1}^{(1)}X_{1j}^{(1)} + X_{iN}^{(1)}X_{Nj}^{(1)}\right)\bar{u}_j \\
&\quad -\tfrac{C_{13}}{C_{33}}\lambda \sum_{j=2}^{N-1} X_{ij}^{(1)}\sigma_{\eta j}, \quad i = 2, \ldots, N-1
\end{aligned} \tag{32}$$

- Clamped-Free (CF)

$$
\begin{aligned}
\frac{d\bar{u}_i}{\mathrm{d}\eta} = \quad & -\lambda \sum_{j=2}^{N} X_{ij}^{(1)} \bar{w}_j + \frac{C_{55}^{(b)}}{C_{55}} \tau_i, \quad i = 2, \ldots, N-1 \\
\frac{d\sigma_{\eta i}}{\mathrm{d}\eta} = \quad & -\frac{\rho}{\rho^{(b)}} \Omega^2 \bar{w}_i - \frac{C_{55}}{C_{55}^{(b)}} \lambda^2 \sum_{j=2}^{N} \left(X_{i1}^{(1)} X_{1j}^{(1)} \right) \bar{w}_j \\
& -\lambda \sum_{j=2}^{N-1} X_{ij}^{(1)} \tau_j, \quad i = 2, \ldots, N \\
\frac{d\bar{w}_i}{\mathrm{d}\eta} = \quad & \frac{C_{13}}{C_{33}} \lambda \sum_{j=2}^{N-1} \left(-X_{ij}^{(1)} + \frac{X_{iN}^{(1)} X_{Nj}^{(1)}}{X_{NN}^{(1)}} \right) \bar{u}_j + \frac{C_{55}^{(b)}}{C_{33}} \sigma_{\eta i} \\
& + \left(\frac{C_{13}}{C_{33}} \right)^2 \left(\frac{\lambda}{\mathrm{A_{CF}}} \frac{X_{iN}^{(1)}}{X_{NN}^{(1)}} \right) \sigma_{\eta N}, \quad i = 2, \ldots, N \\
\frac{d\tau_i}{\mathrm{d}\eta} = \quad & \mathrm{A_{CF}} \lambda \sum_{j=2}^{N-1} \left(-X_{ij}^{(2)} + \frac{X_{iN}^{(2)} X_{Nj}^{(1)}}{X_{NN}^{(1)}} \right) \bar{u}_j - \frac{\rho}{\rho^{(b)}} \Omega^2 \bar{u}_i \\
& - \left(\frac{C_{13}^2}{C_{33}} \frac{\lambda^2}{C_{55}^{(b)}} \right) \sum_{j=2}^{N-1} X_{i1}^{(1)} \left(X_{1j}^{(1)} - \frac{X_{1N}^{(1)} X_{Nj}^{(1)}}{X_{NN}^{(1)}} \right) \bar{u}_j \\
& + \frac{C_{13}}{C_{33}} \lambda \left(\frac{X_{iN}^{(2)}}{X_{NN}^{(1)}} + \left(\frac{C_{13}^2}{C_{33}} \frac{\lambda}{\mathrm{A_{CF}} C_{55}^{(b)}} \right) \frac{X_{1N}^{(1)} X_{i1}^{(1)}}{X_{NN}^{(1)}} \right) \sigma_{\eta N} \\
& - \frac{C_{13}}{C_{33}} \lambda \sum_{j=2}^{N} X_{ij}^{(1)} \sigma_{\eta j}, \quad i = 2, \ldots, N-1
\end{aligned}
\tag{33}
$$

- Free-Free (FF)

$$
\begin{aligned}
\frac{d\bar{u}_i}{\mathrm{d}\eta} = \quad & -\lambda \sum_{j=1}^{N} X_{ij}^{(1)} \bar{w}_j + \frac{C_{55}^{(b)}}{C_{55}} \tau_i, \quad i = 2, \ldots, N-1 \\
\frac{d\sigma_{\eta i}}{\mathrm{d}\eta} = \quad & -\frac{\rho}{\rho^{(b)}} \Omega^2 \bar{w}_i - \lambda \sum_{j=2}^{N-1} X_{ij}^{(1)} \tau_j, \quad i = 1, 2, \ldots, N \\
\frac{d\bar{w}_i}{\mathrm{d}\eta} = \quad & \left(\frac{C_{13}}{C_{33}} \frac{\lambda}{\mathrm{B_{FF}}} \right) \sum_{j=2}^{N-1} (X_{i1}^{(1)} \left(X_{1j}^{(1)} X_{NN}^{(1)} - X_{1N}^{(1)} X_{Nj}^{(1)} \right) \\
& + X_{iN}^{(1)} \left(X_{Nj}^{(1)} X_{11}^{(1)} - X_{1j}^{(1)} X_{N1}^{(1)} \right)) \bar{u}_j - \frac{C_{13}}{C_{33}} \lambda \sum_{j=2}^{N-1} X_{ij}^{(1)} \bar{u}_j \\
& + \left(\frac{C_{13}}{C_{33}} \right)^2 \left(\frac{\lambda}{\mathrm{B_{FF}} \mathrm{A_{FF}}} \right) \Big(\left(X_{i1}^{(1)} X_{NN}^{(1)} - X_{iN}^{(1)} X_{N1}^{(1)} \right) \sigma_{\eta 1} \\
& - \left(X_{i1}^{(1)} X_{1N}^{(1)} - X_{iN}^{(1)} X_{11}^{(1)} \right) \sigma_{\eta N} \Big) + \frac{C_{55}^{(b)}}{C_{33}} \sigma_{\eta i}, \quad i = 1, 2, \ldots, N
\end{aligned}
\tag{34}
$$

$$\frac{d\tau_i}{\mathrm{d}\eta} = \left(\frac{\mathrm{A_{FF}}}{\mathrm{B_{FF}}}\right)\lambda \sum_{j=2}^{N-1} (X_{i1}^{(2)}\left(X_{1j}^{(1)} X_{NN}^{(1)} - X_{1N}^{(1)} X_{Nj}^{(1)}\right)$$
$$+X_{iN}^{(2)}\left(X_{Nj}^{(1)} X_{11}^{(1)} - X_{1j}^{(1)} X_{N1}^{(1)}\right))\bar{u}_i - \mathrm{A_{FF}}\lambda \sum_{j=2}^{N-1} X_{ij}^{(2)}\bar{u}_j$$
$$-\frac{\rho}{\rho^{(b)}}\Omega^2\bar{u}_i + \left(\frac{C_{13}}{C_{33}}\right)\frac{\lambda}{\mathrm{B_{FF}}}(\left(X_{i1}^{(2)} X_{NN}^{(1)} - X_{iN}^{(2)} X_{N1}^{(1)}\right)\sigma_{\eta 1}$$
$$-\left(X_{i1}^{(2)} X_{1N}^{(1)} - X_{iN}^{(2)} X_{11}^{(1)}\right)\sigma_{\eta N}) - \frac{C_{13}}{C_{33}}\lambda \sum_{j=1}^{N} X_{ij}^{(1)}\sigma_{\eta j}, \quad i = 2, \ldots, N-1$$

$$\mathrm{B_{FF}} = \left(X_{11}^{(1)} X_{NN}^{(1)} - X_{1N}^{(1)} X_{N1}^{(1)}\right)$$

- Clamped-simply supported (CS)

$$\begin{aligned}
\tfrac{d\bar{u}_i}{\mathrm{d}\eta} &= -\lambda \sum_{j=2}^{N-1} X_{ij}^{(1)}\bar{w}_j + \tfrac{C_{55}^{(b)}}{C_{55}}\tau_i, \quad i = 2, \ldots, N \\
\tfrac{d\sigma_{\eta i}}{\mathrm{d}\eta} &= -\tfrac{\rho}{\rho^{(b)}}\Omega^2\bar{w}_i - \tfrac{C_{55}}{C_{55}^{(b)}}\lambda^2 \sum_{j=2}^{N-1}\left(X_{i1}^{(1)} X_{1j}^{(1)}\right)\bar{w}_j - \lambda \sum_{j=2}^{N} X_{ij}^{(1)}\tau_j, \quad i = 2, \ldots; N-1 \\
\tfrac{d\bar{w}_i}{\mathrm{d}\eta} &= -\tfrac{C_{13}}{C_{33}}\lambda \sum_{j=2}^{N} X_{ij}^{(1)}\bar{u}_j + \tfrac{C_{55}^{(b)}}{C_{33}}\sigma_{\eta i}, \quad i = 2, \ldots, N-1 \\
\tfrac{d\tau_i}{\mathrm{d}\eta} &= \mathrm{A_{CS}}\lambda \sum_{j=2}^{N}\left(-X_{ij}^{(2)} + X_{iN}^{(1)} X_{Nj}^{(1)}\right)\bar{u}_j - \tfrac{\rho}{\rho^{(b)}}\Omega^2\bar{u}_i \\
&\quad -\left(\tfrac{C_{13}^2}{C_{33}}\tfrac{\lambda^2}{C_{55}^{(b)}}\right)\sum_{j=2}^{N} X_{i1}^{(1)} X_{1j}^{(1)}\bar{u}_j - \tfrac{C_{13}}{C_{33}}\lambda \sum_{j=2}^{N-1} X_{ij}^{(1)}\sigma_{\eta j}, \; i = 2, \ldots, N
\end{aligned} \tag{35}$$

- Simply supported-Free (SF)

$$\begin{aligned}
\tfrac{d\bar{u}_i}{\mathrm{d}\eta} &= -\lambda \sum_{j=2}^{N} X_{ij}^{(1)}\bar{w}_j + \tfrac{C_{55}^{(b)}}{C_{55}}\tau_i, \quad i = 1, 2, \ldots, N-1 \\
\tfrac{d\sigma_{\eta i}}{\mathrm{d}\eta} &= -\tfrac{\rho}{\rho^{(b)}}\Omega^2\bar{w}_i - \lambda \sum_{j=1}^{N-1} X_{ij}^{(1)}\tau_j, \quad i = 2, \ldots, N \\
\tfrac{d\bar{w}_i}{\mathrm{d}\eta} &= \tfrac{C_{13}}{C_{33}}\lambda \sum_{j=1}^{N-1}\left(-X_{ij}^{(1)} + \tfrac{X_{iN}^{(1)} X_{Nj}^{(1)}}{X_{NN}^{(1)}}\right)\bar{u}_j + \tfrac{C_{55}^{(b)}}{C_{33}}\sigma_{\eta i} \\
&\quad +\left(\tfrac{C_{13}}{C_{33}}\right)^2\left(\tfrac{\lambda}{\mathrm{A_{SF}}}\tfrac{X_{iN}^{(1)}}{X_{NN}^{(1)}}\right)\sigma_{\eta N}, \quad i = 2, \ldots, N
\end{aligned} \tag{36}$$

$$\begin{aligned}\frac{d\tau_i}{\mathrm{d}\eta} =& \mathrm{A_{SF}}\lambda\sum_{j=1}^{N-1}\left(-X_{ij}^{(2)}+\frac{X_{iN}^{(2)}X_{Nj}^{(1)}}{X_{NN}^{(1)}}-X_{i1}^{(1)}\left(X_{1j}^{(1)}-\frac{X_{1N}^{(1)}X_{Nj}^{(1)}}{X_{NN}^{(1)}}\right)\right)\bar{u}_j\\ &-\frac{\rho}{\rho^{(b)}}\Omega^2\bar{u}_i+\frac{C_{13}}{C_{33}}\lambda\left(\frac{X_{iN}^{(2)}}{X_{NN}^{(1)}}-\frac{X_{i1}^{(1)}X_{1N}^{(1)}}{X_{NN}^{(1)}}\right)\sigma_{\eta N}\\ &-\frac{C_{13}}{C_{33}}\lambda\sum_{j=2}^{N}X_{ij}^{(1)}\sigma_{\eta j},\quad i=1,2,\ldots,N-1\end{aligned}$$

- Clamped-Guided (CG)

$$\begin{aligned}\tfrac{d\bar{u}_i}{\mathrm{d}\eta} =& -\lambda\sum_{j=2}^{N-1}X_{ij}^{(1)}\bar{w}_j+\tfrac{C_{55}^{(b)}}{C_{55}}\tau_i,\quad i=2,\ldots,N-1\\ \tfrac{d\sigma_{\eta i}}{\mathrm{d}\eta} =& -\tfrac{\rho}{\rho^{(b)}}\Omega^2\bar{w}_i-\lambda^2\tfrac{C_{55}}{C_{55}^{(b)}}\sum_{j=2}^{N}X_{1j}^{(1)}X_{i1}^{(1)}\bar{w}_j-\lambda\sum_{j=2}^{N-1}X_{ij}^{(1)}\tau_j,\quad i=2,\ldots,N\\ \tfrac{d\bar{w}_i}{\mathrm{d}\eta} =& -\tfrac{C_{13}}{C_{33}}\lambda\sum_{j=2}^{N-1}X_{ij}^{(1)}\bar{u}_j+\tfrac{C_{55}^{(b)}}{C_{33}}\sigma_{\eta i},\quad i=2,\ldots,N\\ \tfrac{d\tau_i}{\mathrm{d}\eta} =& -\lambda\sum_{j=2}^{N-1}\left(\mathrm{A_{CG}}X_{i1}^{(2)}+\lambda\tfrac{C_{13}^2}{C_{33}C_{55}^{(b)}}X_{1j}^{(1)}X_{i1}^{(1)}\right)\bar{u}_j-\tfrac{\rho}{\rho^{(b)}}\Omega^2\bar{u}_i\\ &-\tfrac{C_{13}}{C_{33}}\lambda\sum_{j=2}^{N}X_{ij}^{(1)}\sigma_{\eta j},\quad i=2,\ldots,N-1\end{aligned}\tag{37}$$

- Free-Guided (FG)

$$\begin{aligned}\tfrac{d\bar{u}_i}{\mathrm{d}\eta} =& -\lambda\sum_{j=1}^{N}X_{ij}^{(1)}\bar{w}_j+\tfrac{C_{55}^{(b)}}{C_{55}}\tau_i,\quad i=2,\ldots,N-1\\ \tfrac{d\sigma_{\eta i}}{\mathrm{d}\eta} =& -\tfrac{\rho}{\rho^{(b)}}\Omega^2\bar{w}_i-\lambda\sum_{j=2}^{N-1}X_{ij}^{(1)}\tau_j,\quad i=1,2,\ldots,N\\ \tfrac{d\bar{w}_i}{\mathrm{d}\eta} =& \tfrac{C_{13}}{C_{33}}\lambda\sum_{j=2}^{N-1}\left(-X_{ij}^{(1)}+\tfrac{X_{i1}^{(1)}X_{1j}^{(1)}}{X_{11}^{(1)}}\right)\bar{u}_j+\tfrac{C_{55}^{(b)}}{C_{33}}\sigma_{\eta i}\\ &+\left(\tfrac{C_{13}}{C_{33}}\right)^2\left(\tfrac{\lambda}{\mathrm{A_{FG}}}\tfrac{X_{i1}^{(1)}}{X_{11}^{(1)}}\right)\sigma_{\eta 1},\quad i=1,2,\ldots,N\\ \tfrac{d\tau_i}{\mathrm{d}\eta} =& -\mathrm{A_{FG}}\lambda\sum_{j=2}^{N-1}\left(X_{ij}^{(2)}-\tfrac{X_{i1}^{(2)}X_{1j}^{(1)}}{X_{11}^{(1)}}\right)\bar{u}_j-\tfrac{\rho}{\rho^{(b)}}\Omega^2\bar{u}_i\\ &-\tfrac{C_{13}}{C_{33}}\lambda\sum_{j=1}^{N}X_{ij}^{(1)}\sigma_{\eta j}+\left(\tfrac{C_{13}}{C_{33}}\lambda\tfrac{X_{i1}^{(2)}}{X_{11}^{(1)}}\right)\sigma_{\eta j},\quad i=2,\ldots,N-1\end{aligned}\tag{38}$$

The vectors $\boldsymbol{\delta}_0$, $\boldsymbol{\delta}$, $\mathbf{f}$ and matrices $\mathbf{T}$, $\mathbf{J}$ in the equations (18) and (19) are as follows

$$\boldsymbol{\delta}_0 = \begin{Bmatrix} \boldsymbol{\delta}(0)^{(b)} \\ \boldsymbol{\delta}(0)^{(c)} \\ \boldsymbol{\delta}(0)^{(t)} \end{Bmatrix}, \quad \boldsymbol{\delta} = \begin{Bmatrix} \boldsymbol{\delta}(0)^{(b)} \\ \boldsymbol{\delta}(h)^{(b)} \\ \boldsymbol{\delta}(0)^{(c)} \\ \boldsymbol{\delta}(h)^{(c)} \\ \boldsymbol{\delta}(0)^{(t)} \\ \boldsymbol{\delta}(h)^{(t)} \end{Bmatrix}, \quad \mathbf{f} = \begin{Bmatrix} \mathbf{f}^{(b)} \\ \mathbf{0} \\ \mathbf{0} \\ \mathbf{f}^{(t)} \end{Bmatrix} \tag{39}$$

$$\mathbf{T} = \begin{bmatrix} \mathbf{T}^{(b)} & \mathbf{0} & \mathbf{0} \\ \mathbf{0} & \mathbf{T}^{(c)} & \mathbf{0} \\ \mathbf{0} & \mathbf{0} & \mathbf{T}^{(t)} \end{bmatrix}, \quad \mathbf{J} = \begin{bmatrix} \mathbf{J}^{(b)} & \mathbf{0} & \mathbf{0} & \mathbf{0} \\ \mathbf{0} & \mathbf{J}^{(\mathrm{I})} & \mathbf{0} & \mathbf{0} \\ \mathbf{0} & \mathbf{0} & \mathbf{J}^{(\mathrm{I})} & \mathbf{0} \\ \mathbf{0} & \mathbf{0} & \mathbf{0} & \mathbf{J}^{(t)} \end{bmatrix}$$
$$\text{where, } \mathbf{J}^{(t)} = \mathbf{J}^{(b)} = \begin{bmatrix} \mathbf{0} & \mathbf{i} & \mathbf{0} & \mathbf{0} \\ \mathbf{0} & \mathbf{0} & \mathbf{0} & \mathbf{i} \end{bmatrix}, \quad \mathbf{J}^{(\mathrm{I})} = \begin{bmatrix} \mathbf{I} & -\mathbf{I} \end{bmatrix} \tag{40}$$
$$\mathbf{f}^{(t)} = \begin{Bmatrix} \mathbf{f}_\sigma \\ \mathbf{f}_\tau \end{Bmatrix}^{(t)}, \mathbf{f}^{(b)} = \begin{Bmatrix} \mathbf{f}_\sigma \\ \mathbf{f}_\tau \end{Bmatrix}^{(b)}$$

2D plane strain constitutive relations for an isotropic material

$$\begin{array}{ll} C_{11} = \frac{(1-\mu)\mathrm{E}}{(1+\mu)(1-2\mu)} & C_{33} = \frac{(1-\mu)\mathrm{E}}{(1+\mu)(1-2\mu)} \\ C_{13} = \frac{\mu \mathrm{E}}{(1+\mu)(1-2\mu)} & C_{55} = \frac{\mathrm{E}}{2(1+\mu)} \end{array} \tag{41}$$

where E is the Young's modulus and μ is the Poisson's ratio.